TRIBHUVAN UNIVERSITY
INSTITUTE OF ENGINEERING
PULCHOWK CAMPUS

B-08-BAS-2019/24

SOUNDING ROCKET FOR ATMOSPHERIC STUDIES

By:
Mridul Neupane (076BAS021)
Nischal Shrestha (076BAS024)
Prashant Giri (076BAS029)
Sunil Khadka (076BAS043)

A PROJECT REPORT TO THE DEPARTMENT OF MECHANICAL AND AEROSPACE ENGINEERING IN PARTIAL FULFILLMENT OF THE REQUIREMENT FOR THE BACHELOR'S DEGREE IN AEROSPACE ENGINEERING

DEPARTMENT OF MECHANICAL AND AEROSPACE ENGINEERING
LALITPUR, NEPAL

March, 2024

COPYRIGHT

TRIBHUVAN UNIVERSITY
INSTITUTE OF ENGINEERING
PULCHOWK CAMPUS
DEPARTMENT OF MECHANICAL AND AEROSPACE ENGINEERING

LETTER OF APPROVAL

The undersigned certify that they have read, and recommended to the Institute of Engineering for acceptance, a project report entitled **"Sounding Rocket for Atmospheric Studies"** submitted by **Mridul Neupane, Nischal Shrestha, Prashant Giri and Sunil Khadka** in partial fulfillment of the requirements for the Bachelor's Degree in Aerospace Engineering.

Supervisor: **Sudip Bhattrai (PhD)**
Assistant Professor
Department of Mechanical and Aerospace Engineering
Institute of Engineering, Pulchowk Campus

External Examiner: **Er. Sanjiv Paudel**
Managing Director
Machine Hub Nepal

Tribhuvan University
Institute of Engineering
Department of Mechanical and Aerospace Engineering
Pulchowk Campus

Head of Department : **Sudip Bhattrai (PhD)**
Assistant Professor
Department of Mechanical and Aerospace Engineering
Institute of Engineering, Pulchowk Campus

13th March, 2024

DATE OF APPROVAL:

ACKNOWLEDGEMENT

We extend our sincere gratitude to the esteemed faculty members and instructors of the Department of Mechanical and Aerospace Engineering at Pulchowk Campus for their consistent support, guidance, and motivation during this project.

Special thanks are due to our supervisor, Dr. Sudip Bhattrai, whose mentorship and insightful direction have been invaluable. His expertise significantly contributed to refining and improving the quality of our work. We also acknowledge Asst. Prof. Kamal Darlami and Asst. Prof. Aashish Karki for their valuable insights over the past year.

Our gratitude also goes to the Robotics Club, IOE Pulchowk, and the Workshop Technology Laboratory for generously providing us with access to their resources and facilities, which played a vital role in executing the practical aspects of our project.

We express heartfelt thanks to the Incubation, Innovation, and Entrepreneurship Center (IIEC) for providing us with a conducive workspace, facilitating our collaborative efforts and idea implementation. Additionally, we would like to acknowledge our senior, Er. Anup Pandey, for his consistent guidance throughout the duration.

Additionally, we appreciate the assistance of Mr. Ram Prasad Chaudhary, mayor of Kolhabi Municipality, Bara, Nepal, and Mr. Rohit Shiwakoti for their support with the test site and facilities. Special thanks to Tamagadhi Event Venue, Kolhabi, for providing us with a workspace.

Finally, we acknowledge the SRB Team of IOE Pulchowk for their unwavering assistance and support, which significantly contributed to the progress of our project. We particularly thank Sashakta Kharel and Prabin Bhattarai for their continuous help. Our gratitude extends to our friends, seniors, and juniors who have been part of this journey and contributed to the achievement of our project goals.

Mridul Neupane (076BAS021)
Nischal Shrestha (076BAS024)
Prashant Giri (076BAS029)
Sunil Khadka (076BAS043)

ABSTRACT

Sounding rockets hold a critical role in atmospheric exploration by facilitating the gathering and examination of various atmospheric factors like temperature, pressure, humidity, and chemical composition. The primary objective of this project is to conduct tests on the payload deployment system within a sounding rocket. The key challenges include developing a motor that is safe, reliable, and consistently performs as expected, as well as creating a recovery system, such as parachute deployment, capable of withstanding the demanding conditions of launch and subsequent high-speed or high-altitude flight. The study centers on the comprehensive design and development of rockets from scratch, encompassing the propulsion system, motor, and propellant, as well as the recovery system featuring a deployment mechanism and parachute, all built entirely from the ground up. Additionally, fully constructed avionics and payload systems are included. Specifically, a propulsion system capable of hoisting an 8-kilogram vehicle to an altitude of 1000 meters has been designed and manufactured, with the potential for further enhancements to increase altitude capabilities. Moreover, a versatile vehicle capable of conducting missions involving payload deployment and achieving full recovery with a built-in parachute deployment mechanism has been constructed.

Keywords: Sounding rockets, Payload deployment, Recovery system, Propellant

TABLE OF CONTENTS

List of Figures

List of Tables

LIST OF ABBREVIATIONS

AoA	Angle of Attack
O/F	Oxygen to Fuel Ratio
KNSU	Potassium Nitrate-Sucrose
MOC	Method of Characteristics
CG	Center of Gravity
CP	Center of Pressure
CAAN	Civil Aviation Authority of Nepal
MOHA	Ministry of Home Affairs
LoRa	Long Range
BEM	Ballistic Evaluation Motor
BMP	Barometric Pressure
ESP	Embedded System Platform
MPU	Motion Processing Unit
PMS	Particulate Matter Sensor
DHT	Digital Humidity and Temperature Sensor
GPS	Global Positioning System
CNC	Computer Numerical control
PCB	Printed Circuit Board
PVC	Polyvinyl chloride
GSM	Global System for Mobile Communications
SD	Secure Digital
TPU	Thermoplastic polyurethane

LIST OF SYMBOLS

C_m	Coefficient of moment
C_d	Coefficient of drag
$\mathscr{M}$	Molecular mass
γ	Ratio of specific heat
C_p	Specific heat capacity at constant pressure
C_v	Specific heat capacity at constant temperature
r	Burn rate of fuel
a	Velocity of sound
α	Burn rate of solid propellant
n	pressure exponent
$\dot{m}$	Mass flow rate
v_e	Exit velocity at nozzle
A_e	Area of the outlet of nozzle
p_e	Exit pressure at the nozzle outlet
p_a	Ambient pressure
g_0	Acceleration due to gravity
I_{sp}	Specific impulse of a rocket
A^*	Area of throat at sonic flow
R	Universal gas constant
T	Absolute temperature
T_0	Stagnation temperature
p_0	Stagnation pressure
p_c	Chamber pressure
ρ_0	Density of air
A_t	Area of throat of nozzle
M	Mach number
h_0	Stagnation or total enthalpy
h_e	Static enthalpy at nozzle exit
p_e	Static pressure at nozzle exit
p_t	Pressure at throat of nozzle
T_t	Temperature at throat of nozzle
ρ_t	Temperature at throat of nozzle
v_t	Terminal velocity of parachute
A_b	Area of burning surface of grain

CHAPTER 1: INTRODUCTION

1.1. Background

Sounding rockets are small-scale rockets designed specifically for research objectives involving atmospheric data collection and analysis. The concept of sounding rockets dates back to the early 20^{th} century when scientists search for a means to investigate the upper atmosphere and its properties. They are generally being used for global communications and information transfer, weather, climate and environmental observation and forecasting, remote-sensing/observation of the universe, and investigating space physics phenomenon[1]. Sounding rockets have become invaluable tools in scientific exploration, providing a cost-effective alternative to satellite-based observations.
Sounding rockets have been employed to deploy a wide range of payloads including scientific instruments and experiments. Instruments carried on these rockets help to collect data on atmospheric properties at different altitudes, such as temperature, pressure, humidity, and chemical composition. This data provides insights into atmospheric dynamics, climate patterns, and the behavior of air pollutants, contributing to a better understanding of Earth's atmosphere and its impact on our planet.

1.2. Objectives

The main objective of the project is to perform atmospheric studies using a sounding rocket.

The specific objectives of the project are:

- To design and fabricate systems capable of carrying out missions.
- To characterize the propellant based on composition and conduct static tests.
- To perform flight tests and collect atmospheric data.

1.3. Problem Statement

Nepal does not currently have a specific system for measuring atmospheric data, which limits the country's capacity to carry out research and experiments in the areas of exploration, atmospheric studies, and technological innovation. Weather balloons have

been the standard method for data collection up to this point since the unpredictable travel of data makes system recovery expensive and impractical. Therefore, there are constraints and difficulties in the realm of assessing atmospheric data. As the course is predictable, the measurement device can be retrieved, and there is financial savings, employing sounding rockets can optimize the capability for gathering superior, high-resolution atmospheric observations.

1.4. Feasibility Analysis

1.4.1. Economic Feasibility

Various factors influence the cost of launching a sounding rocket for atmospheric data assessment. The size of the payload, altitude requirements, mission duration, instrumentation for rocket production and testing, and number of sensors for data acquisition are some of the major factors that determine the cost of launching a sounding rocket. Securing funds and a cost-effective mission plan is required for the economic feasibility of the project.

1.4.2. Technical Feasibility

The development of sounding rockets has a well-established technical foundation. The required technologies for atmosphere data collection like sensors to measure atmospheric data and communication between sounding rockets and ground stations are available. This demonstrates the availability of technical resources for this project.

1.4.3. Operational Feasibility

The operation of a sounding rocket requires various secondary instruments including launch pads, safety measures, a ground control station, and other testing equipment like a thrust stand and pressure chamber. Safety protocols and regulations are of utmost importance during the production, testing, and launching stage of a sounding rocket. Sounding rocket launches must take place away from residential areas as designated by the regulation protocol.

CAAN plays a vital role in ensuring the safe and efficient operation of rocket activities in Nepal. To conduct rocket operations, obtaining regulations and permissions from CAAN is crucial. This includes acquiring a Rocket Launch Permit, which outlines launch specifics and ensures compliance with safety regulations. CAAN conducts

a comprehensive safety assessment, considering factors like launch trajectory and potential impact on surrounding areas. This assessment aims to identify and mitigate any risks associated with the launch, prioritizing safety for airspace users and the public. Additionally, CAAN may review the payload, especially if it contains hazardous materials or sensitive components, to ensure compliance with national and international transportation regulations. Adhering to these regulations guarantees the safety and security of the entire launch operation.

MOHA's role in Nepal encompasses public safety, security, and emergency management. Depending on the project, obtaining specific regulations and permissions from MOHA may be necessary. This can involve acquiring security clearances for project personnel, ensuring their reliability and protecting sensitive information. Coordination with law enforcement agencies may also be required to address security concerns and establish appropriate security measures. Adhering to MOHA's safety regulations is essential for maintaining a safe operational environment, including protocols for handling hazardous materials and emergency response plans. By complying with these requirements, the project demonstrates its commitment to public safety and security.

1.5. System Requirement

1.5.1. Software Requirement

Table 1.1: Software Applications

Software	Applications
MATLAB	Calculations, graphs
CATIA V5 and SolidWorks	CAD Design
OpenRocket	Rocket Design and Simulation
RASAero II	Aerodynamic Analysis, Stability and control analysis, trajectory simulation, performance optimization, data visualization
Arduino IDE	Flight computer, Data acquisition
OpenMotor	Internal Ballistics Simulation
ProPrep	Propellant Analysis
BurnSim	Determination of Kn, Estimated Chamber Pressure, performance of solid motor
RDWorks	Laser Cutting and Engraving

1.5.2. Hardware Requirement

Table 1.2: Hardware Applications

Hardware	Applications
3D Printer	Nose cone, Various Components
Sensors	Sensors: Data measurement (Temperature Sensors, Pressure Sensors, GPS Module, Pollutant Sensors)
Milling Machine CNC Laser Cutters Lathe Machine	Nozzle, Shafts, Motor Bulkheads, components fabrication

CHAPTER 2: LITERATURE REVIEW

Sounding rockets are unique, unmanned, and cost-effective experimental platforms for in-situ measurements in all atmospheric layers and space. They offer real-time data transmission, telecommand interaction, and parachute recovery for reusable payloads. Unlike aircraft or balloons, rockets are essential for studying middle atmosphere phenomena at meaningful scales through in-situ measurements, as remote sensing technologies cannot currently substitute these measurements[1].

The selection of propellant for rocket motors is crucial, and several key characteristics must be considered. These include high performance (specific impulse), predictable burning rate, consistent thrust and chamber pressure, suitable physical properties, high density, reliable ignition qualities, good aging characteristics, low moisture absorption, safe and cost-effective manufacturing, low technical risk, insensitivity to certain energy stimuli, non-toxic exhaust gases, and combustion stability. Considering these factors ensures the propellant meets the requirements for performance, reliability, safety, and manufacturability[2].

Lucas de Almeida Sabino Carvallho et al. (2019): calculated and analysed the drag forces due to different shapes of nose cone of the rocket. This paper employs computational fluid dynamics analysis to determine the most aerodynamically efficient rocket nose cone design for academic rockets, focusing on lower drag force across various velocities, accounting for boundary layer effects and turbulence[3]. Shapes examined include tangent ogive, parabolic ogive, ellipsoidal ogive, and conical shapes. Mach numbers range from 0.05 to 0.62. Results indicate that elliptical and tangent ogive shapes exhibit superior aerodynamic properties, followed by the parabolic shape, while the conical shape experiences the most drag. Elliptical shapes are recommended for subsonic flights, while parabolic or tangent shapes are suggested for supersonic missions.

S. S. Sankalp et al. (2022) conducted a computational analysis on various tail configurations for sounding rockets. The study focused on fins with cant angles, commonly used to minimize instability by providing a rolling moment. Aerodynamic coefficients like C_d and C_m were examined with different angles of attack (AoA). Both trapezoidal and elliptical fins showed increased drag coefficients with higher AoA and cant angles. Increasing cant angle raised the rolling moment coefficient for both fin types at a constant aspect ratio. The trapezoidal configuration demonstrated a higher C_m/C_d ratio than the elliptical one, especially at higher aspect ratios, making it the optimal choice despite

experiencing higher drag[4].

Knacke provides a comprehensive examination of parachute design principles and engineering techniques. Knacke's manual explores various aspects of parachute recovery systems, including aerodynamics, materials, and deployment mechanisms. The review highlights the book's significance in providing practical insights for designing effective parachute systems, making it a valuable resource for engineers, researchers, and enthusiasts in the field[5].

CHAPTER 3: THEORETICAL BACKGROUND

3.1. Propellant Theory

Sounding rockets mostly use solid propellant as fuel for the engine. The solid propellant possess certain very definite advantages which make them attractive to users because of their simplicity, which are either prepackaged or cast directly into the rocket motor, and do not require the elaborate plumbing and control mechanisms that the liquid propellant which gives them a practical advantage of prime importance [7].

3.1.1. Composition of Propellant

The composition of the propellant is selected upon the basis of availability of the constituents, cost, safety, castability, consistency of performance, and adequate performance. The propellant is composed of Sucrose as fuel and Potassium Nitrate as the oxidizer. The standard ratio of constituents for KNSU is 65 percent Potassium Nitrate and 35 percent Sucrose, by mass. This ratio has proven to give the best overall performance combined with acceptable casting qualities. The combustion temperature rises sharply with increased O/F ratio. At the 65/35 ratio, steel nozzles suffer little or no erosion, as there is an adequate margin between the theoretical flame temperature (1450°C) and the melting point of steel (approx. 1500°C). At higher O/F ratios, this margin is reduced such that a small error in weighing during preparation could result in a heat damaged nozzle. The standard O/F ratio of 65/35 is not pourable, and must be scooped into the casting mould[8].

3.1.2. Combustion

A rocket motor operates on the basic principle of converting heat energy, from chemical reactions, to kinetic energy. In other words, the heat liberated by the combustion of propellant supplies the heat energy; the high velocity exhaust products exiting the motor have gained kinetic energy. This is why the exhaust experiences a significant drop in temperature as it flows through the nozzle, a requirement of the thermodynamics law of ”conservation of energy”.

$$C_{12}H_{22}O_{11} + 6.29KNO_3 \rightarrow 3.80CO_2 + 5.21CO + 7.79H_2O + 3.07H_2 + 3.14N_2 + 3.00K_2CO_3 + 0.27KOH$$

The performance of the rocket is based upon the combustion ratio and the exhaust gaseous properties of products. The average molecular mass of the products is given by:

$$\mathscr{M}_{avg} = \frac{Y_i\mathscr{M}_i + Y_j\mathscr{M}_j + Y_k\mathscr{M}_k + ...}{Y_t} \tag{3.1}$$

where $\mathscr{M}_{avg}$ is the average molecular mass, Y_i, Y_j, Y_k are the individual mass ratio of the constituent gases, $\mathscr{M}_i$, $\mathscr{M}_j$, $\mathscr{M}_k$ are the individual molecular mass and Y_t is the total mass ratio whose value is equal to unity.

The ratio of specific heats, γ is another property of the mixture of product gases.

$$\gamma = \frac{C_p}{C_v} \tag{3.2}$$

The value of γ can be determined by the average values of individual constituents.

$$\gamma = \frac{C_p}{C_p - R} \tag{3.3}$$

where R is the universal gas constant.

$$C_p = \frac{Y_iC_{p_i} + Y_jC_{p_j} + Y_kC_{p_k} + ...}{Y_t} \tag{3.4}$$

3.1.3. Relation of Burn Rate v/s Chamber Pressure

Another important parameter of the propellant is the generalization of properties relating the burn rate at the given chamber pressure which is given by,

$$r = \alpha.P^n \tag{3.5}$$

where α is the pressure coefficient and n is the pressure exponent which determine the overall variation of one property with respect to the change in another. P represents the combustion chamber pressure and r represents the burn rate of the fuel. To determine the values, initially the burn rate of the propellant is determined at different chamber pressure and plotted in a graph. With the curve traced with the data points, the values of α and n can be determined.

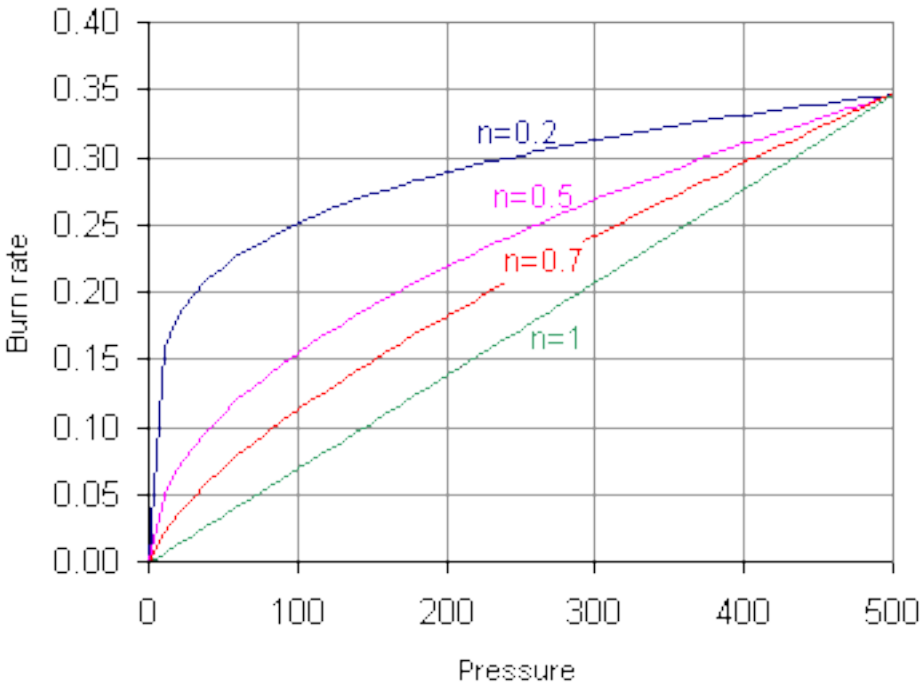

Figure 3.1: Saint Robert's model of burn rate v.s. pressure
[8]

3.1.4. Propellant Grain

A cylindrical grain refers to a type of propellant grain where the internal cross-section remains constant along its axis, regardless of the shape of perforations. Perforations are the central cavities or flow passages within a propellant grain, which can have different shapes such as cylindrical, tubular, rod, or star-shaped. The most commonly used grain type is end-burning, where the propellant burns from one end. During motor burn time, neutral burning occurs when the thrust, pressure, and burning surface area remain relatively constant. Progressive burning refers to a burn time where the thrust, pressure, and burning surface area increase, while regressive burning describes a burn time where these parameters decrease. A stoichiometric mixture is one with the correct proportions of fuel and oxidizer for complete combustion, and the balance of oxygen determines whether the propellant is under-oxidized or over-oxidized. At the end of burning, any unburned propellant remaining or expelled through the nozzle is referred to as a sliver.

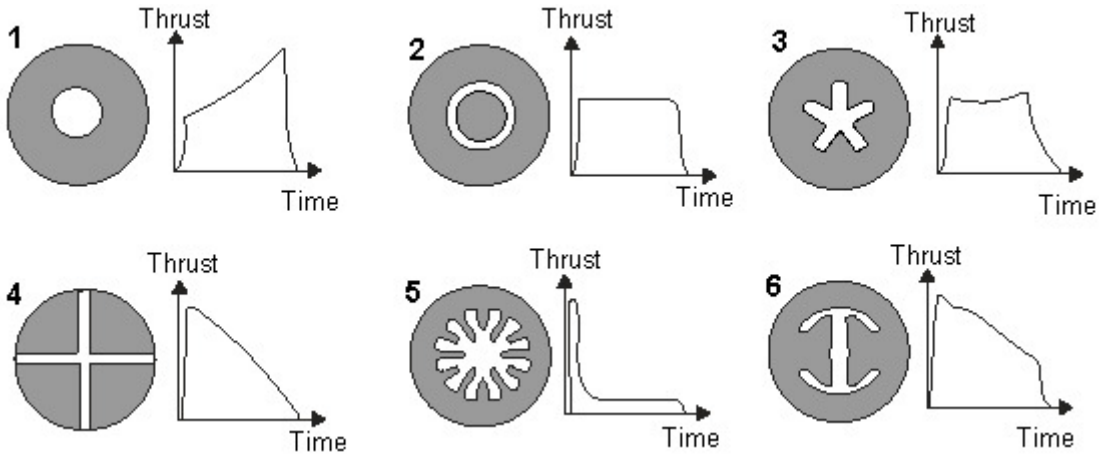

Figure 3.2: Thrust Profile for Different Grains Cross Section
[9]

3.2. Nozzle Theory

The amount of thrust produced by the rocket is given as:

$$F = \dot{m}.v_e + A_e.(p_e - p_a) \tag{3.6}$$

Here, the first term represents the momentum thrust and the second term represents the pressure thrust. The specific impulse of a rocket is given as:

$$I_{sp} = \frac{F}{\dot{m}.g_0} \tag{3.7}$$

where,
g_0= 9.81 m/s^2
The mass flow rate:

$$\dot{m} = \rho.a_t.A_t = constant \tag{3.8}$$

or,

$$\dot{m} = \frac{P_0.A^*}{\sqrt{T_0}}.\sqrt{\frac{\gamma}{R}.(\frac{2}{\gamma+1})(\frac{\gamma+1}{\gamma-1})} \tag{3.9}$$

The velocity of the sound and Mach number:

$$a = \sqrt{\gamma.R.T} \tag{3.10}$$

$$M = \frac{v}{a} \tag{3.11}$$

The isentropic relations are:

$$\frac{T_0}{T} = [1 + \frac{\gamma - 1}{2} M^2] \tag{3.12}$$

$$\frac{p_0}{p} = [1 + \frac{\gamma - 1}{2} M^2]^{\frac{\gamma}{\gamma - 1}} \tag{3.13}$$

$$\frac{\rho_0}{\rho} = [1 + \frac{\gamma - 1}{2} M^2]^{\frac{1}{\gamma - 1}} \tag{3.14}$$

The ratio of the local area to the throat area i.e. area mach relation is given as:

$$\frac{A}{A_t} = \frac{1}{M} [\frac{2}{\gamma + 1} (1 + \frac{\gamma - 1}{2} M^2)]^{\frac{\gamma + 1}{2(\gamma - 1)}} \tag{3.15}$$

The mach number is the function of area ratio[10].
In function of pressure ratio, this can be written as:

$$\frac{A}{A_t} = (\frac{\gamma + 1}{2})^{\frac{1}{\gamma - 1}} (\frac{P_e}{P_0})^{\frac{1}{\gamma}} \sqrt{(\frac{\gamma + 1}{\gamma - 1} [1 - (\frac{P_e}{P_0})^{\frac{\gamma - 1}{\gamma}}]} \tag{3.16}$$

3.3. Parachute Design

The equations used to evaluate, analyse, select and design parachute recovery systems was described by Knacke et al. (1991).
The drag force D generated by a parachute is:

$$D = \frac{1}{2} C_d \rho {v_t}^2 A \tag{3.17}$$

The gravitational force on the rocket and drag force on the parachute are balanced,

$$m_z g = D = \frac{1}{2} C_d \rho {v_t}^2 A \tag{3.18}$$

The impact velocity is chose to be in window of 6 to 10m/s.Then, the diameter of the fully inflated parachute is given as:

$$d = \sqrt{\frac{8 m_z g}{\pi . C_d . {V_t}^2}} \tag{3.19}$$

The mass m_z can be defined as:

$$m_z = m + m_e - m_p \tag{3.20}$$

where, m is the mass of rocket, m_e is the mass of the rocket engine and m_p is the mass of propellant.

3.4. Stability Theory

When developing a new rocket, ensuring its stability becomes a crucial factor. Even a slight disturbance, such as a gust of wind, can cause the rocket to deviate from its original orientation. This deviation results in the rocket flying at an angle of attack (α), where α represents the angle between the rocket centerline and its velocity vector.

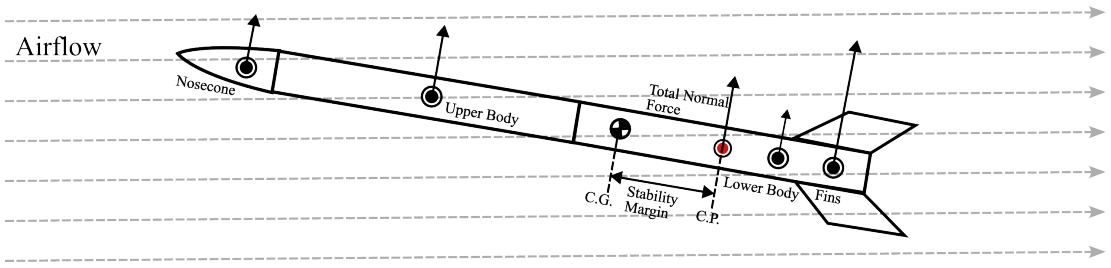

Figure 3.3: Forces in a Rocket Body

In the presence of an angle of attack, the fins of a stable rocket generate a corrective moment to realign the rocket's flight. This corrective moment is produced by aerodynamic forces perpendicular to the rocket's axis. Each component of the rocket contributes a distinct normal force component originating from the component's Center of Pressure (CP), as illustrated in Figure 3.3.

Combining the separate normal forces into a single force, whose magnitude is the sum of the individual forces, results in a force acting at the center of pressure on the rocket. This total force creates a moment attempting to correct the rocket's flight only if the CP is positioned aft (behind) the Center of Gravity (CG). A statically stable rocket, one meeting this condition, consistently generates a corrective moment when flying at a small angle of attack.

The argument for static stability may face challenges in two scenarios: first, if normal forces cancel each other out exactly, producing a moment with zero total force, and second, if the normal force at the CP is in the wrong direction (downward), leading to an uncorrective moment. However, it is emphasized that the only component producing a downward force is a boattail, and this force is equivalent to the associated broadening

of the body. Consequently, the total force acting on the rocket cannot be zero nor in a direction that produces an uncorrective moment when aft of the CG.

$$Stability = \frac{CG - CP}{Diameter} \tag{3.21}$$

The stability margin of a rocket is defined as the distance between the CP and CG, measured in calibers, where one caliber is the maximum body diameter of the rocket. A common guideline among model rocket enthusiasts suggests that the CP should be approximately 1-2 calibers aft of the CG. However, it is noted that the CP of a rocket typically shifts upward as the angle of attack increases, and a 1-2 caliber stability margin may diminish at relatively small angles of attack, termed wind-caused instability due to side winds.

Dynamic stability is another concern for rocketeers, even if a rocket is statically stable. Dynamic instability issues arise over time during a rocket's flight, depending on its shape, size, and mass. These issues include insufficient oscillation damping, too small a corrective moment (over-damped oscillation), and roll-pitch coupling, where natural roll frequency and oscillation frequency may coincide, leading to instability. However, dynamic stability issues are not further considered in this thesis, and an analytical examination of the problem is recommended for a comprehensive understanding.

CHAPTER 4: METHODOLOGY

The assignment was divided into three stages. Initially, the focus was on developing the propulsion system, measuring thrust through static tests, designing systems, and conducting tests on components such as avionics and recovery systems. The subsequent phase involved constructing various components, including the payload, avionics, recovery systems, and propulsion systems integrated with the airframe structure, ultimately leading to the creation of the model rocket. The final stage entailed carrying out flight tests and recovering the rocket. Data collected during these tests were then processed to derive additional results, including air data and flight data.

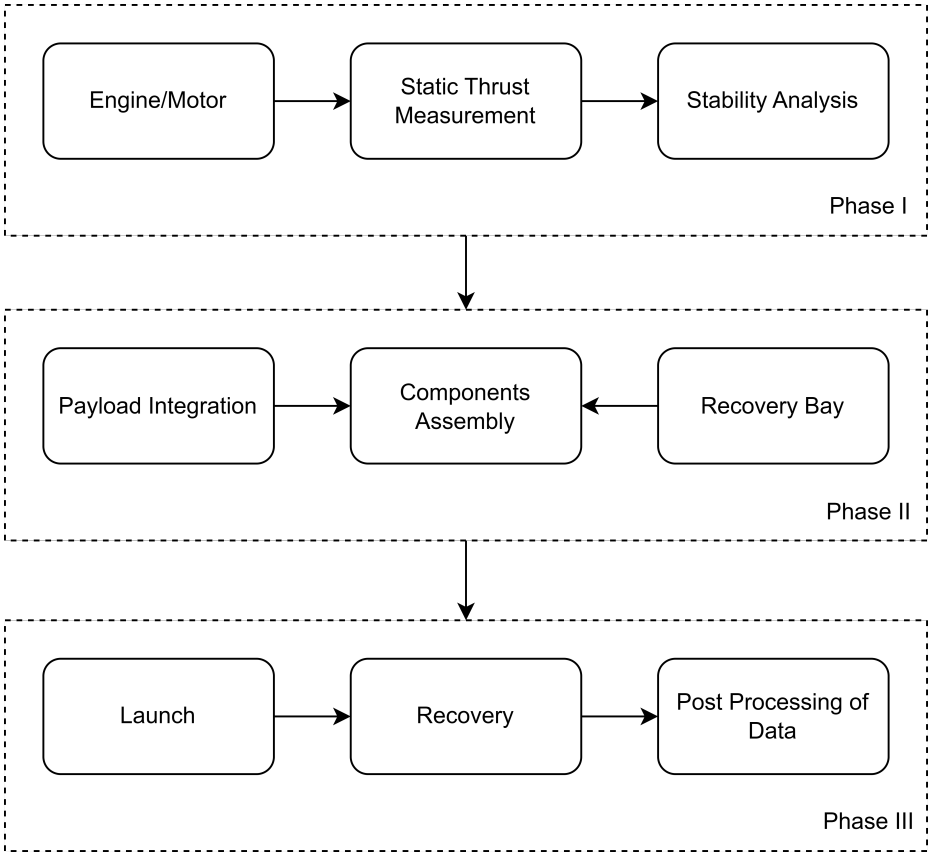

Figure 4.1: Methodology Chart

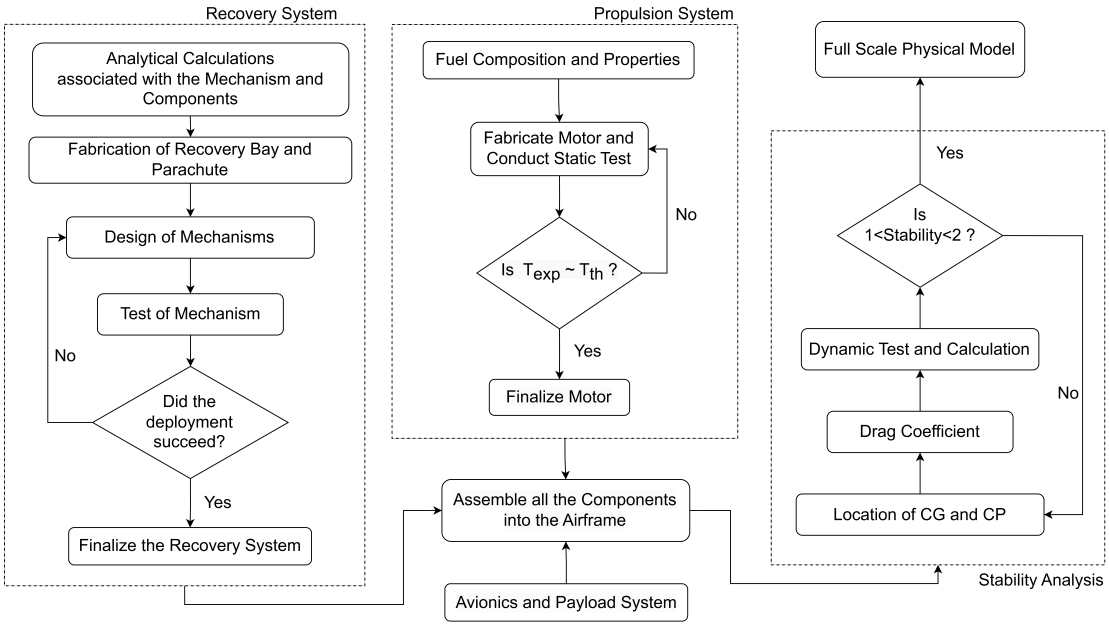

Figure 4.2: Detailed Methodology Chart

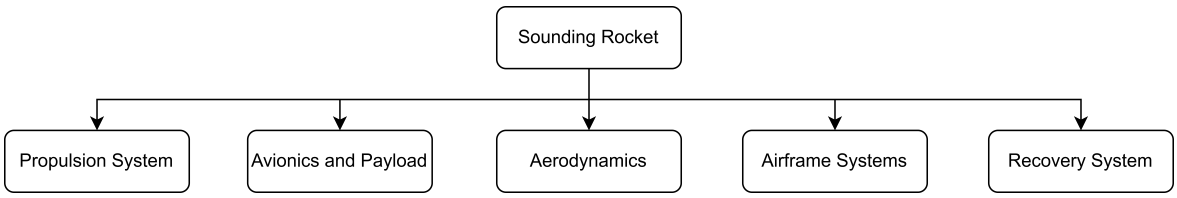

Figure 4.3: Components of Sounding Rocket

4.1. Propulsion System

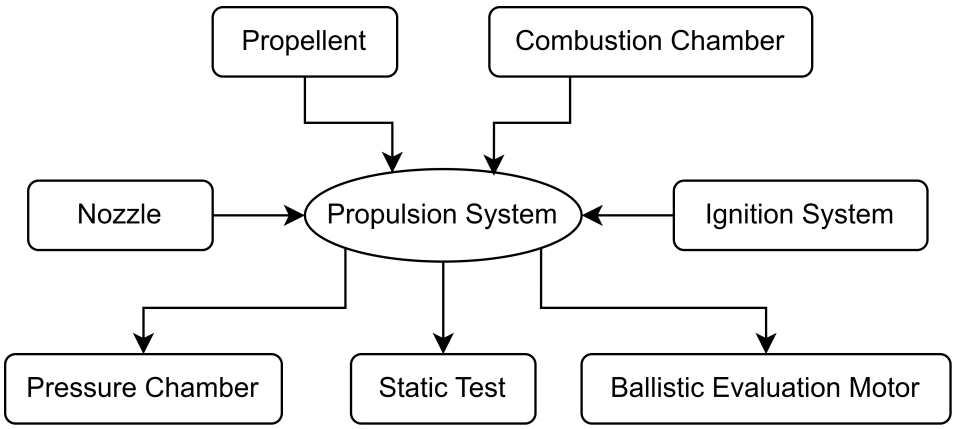

Figure 4.4: Components of Propulsion System

4.1.1. Propellant

The propellant comprised a fused mixture of Potassium Nitrate (KNO_3) serving as the oxidizer, and sucrose (table sugar) serving as the fuel and binder. The standard composition of KNSU's ingredients was 35% sucrose and 65% potassium nitrate by mass. In our case, a 65/35 ratio produced the best performance, with the average specific impulse of 110s. The available propellant characterization data had been mainly obtained for the 65/35 ratio and can be used as the benchmark values for comparison.

Casting and Preparation

In the process of preparing propellant, the initial step involved calculating the required amounts of potassium nitrate (KNO_3) and sucrose ($C_{12}H_{22}O_{11}$) based on specific performance criteria for the rocket. These ingredients were then combined in a saucepan, and just enough water was added to enable the dissolution of KNO_3 and sugar. The mixture was carefully heated, progressing through distinct stages such as boiling, bubbling, and spitting, ultimately reaching a smooth, putty-like consistency. This method prevented caramelization in the saucepan, providing a longer window for packing the propellant into rocket motors. Following the heating process, the propellant needed to be packed into the mold rather than poured and scooped.

Figure 4.5: Propellant Grain

Safety Measure

The KNSU propellant over the years had proven to be safe[8]. However, there were some hazards, and the following precautions were taken:

- The propellant mixture was cooked with thermostatically controlled induction, as the propellant was highly intolerant of overheating.
- The plumes generated during cooking posed a hazard, necessitating the mandatory use of safety glass and masks to ensure proper protection.
- Safety measures during casting included wearing gloves for protection. Water was kept nearby to quickly extinguish any mishap by absorbing heat from the fuel.
- The leftovers were discarded by dissolving in the hot water. The resulting solution was not harmful.

4.1.2. Combustion Chamber

The combustion chamber served as the tube where the combustion process occurs. Given the cylindrical shape of the motor, it required a cylindrical pipe for the chamber, incorporating essential attachments for both the nozzle and engine block. During combustion, the fuel generated a substantial amount of pressure. The combustion chamber must endure the pressure resulting from the combustion process and the use of the nozzle.

With no constraints on weight and considering budget limitations, both mild steel and stainless steel pipes were evaluated. However, mild steel exhibited corrosion due to the byproducts of combustion. Consequently, a stainless steel pipe was chosen for the combustion chamber due to its corrosion resistance, allowing for multiple uses, and its ability to withstand pressure more effectively compared to mild steel. The chosen pipe had an inner diameter of 48 mm with a thickness of 2 mm, resulting in an outer diameter of 52 mm.

Figure 4.6: Stainless Steel Tube as Combustion Chamber

The design pressure of the chamber was 564 psi. For this pressure, the structural analysis of the chamber was done. For the given dimensions of the chamber, maximum stress observed was $4.6477 * 10^7$ pascal with the factor of safety of 12.

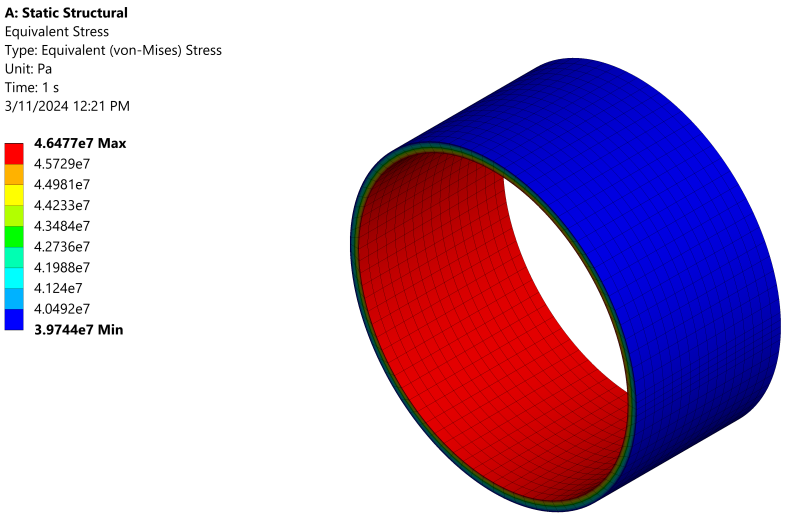

Figure 4.7: Distribution of equivalent (Von Mises) stress on the Combustion Chamber

4.1.3. Nozzle

Initially, due to the absence of evaluated burn rate data for our propellant, we relied on the data (α = 0.156 and n = 0.319) given by the Richard Nakka for the reference. The initial temperature was taken as the auto ignition temperature i.e. 350°C. The web regression and mass flow rate was calculated determining the required diameter of throat for the design pressure of 550 psi. The nozzle dimensions were outlined in the figure 4.9. Although the resulting nozzle produced a flow that was under-expanded, the thrust of 671 N produced was sufficient for phase I flight.

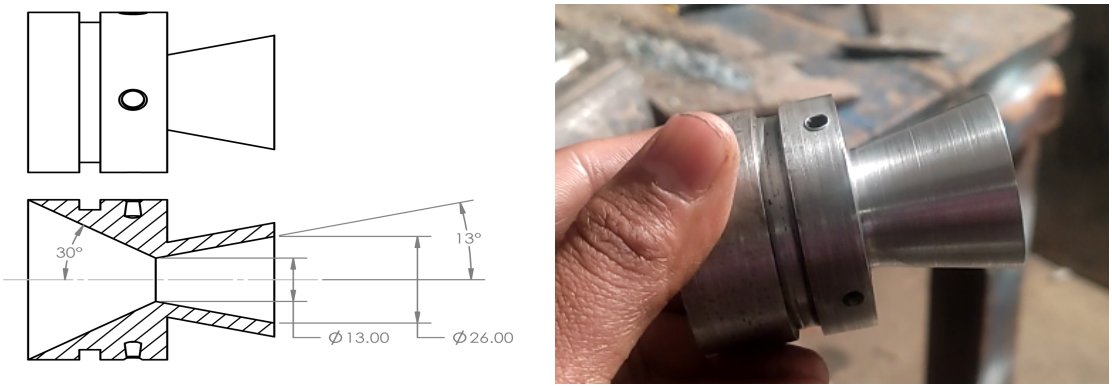

(a) (b)

Figure 4.8: Nozzle (Phase I Motor)

The diameter of combustion chamber was increased for the motor of the phase II flight in order to increase the maximum thrust and burn time. The design pressure of the nozzle initially was chosen as 900 psi with the theoretical peak thrust of 1565 N.
Different lathe operation such as facing, tapering, turning, boring, and parting were carried out in the machining of the nozzle.

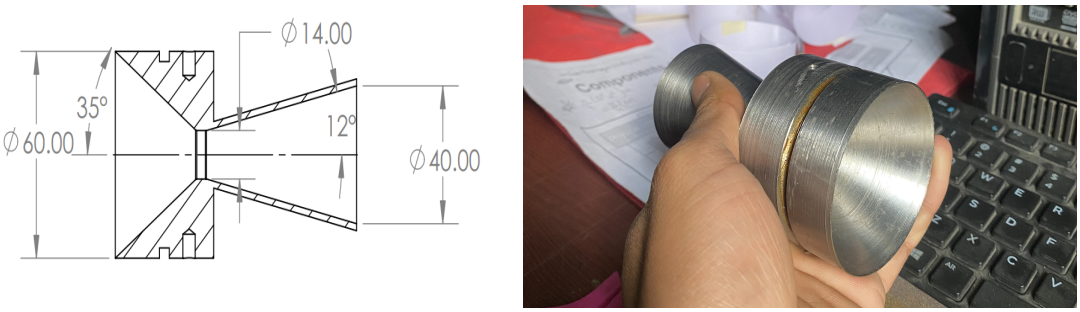

(a) (b)

Figure 4.9: Nozzle (Phase II Motor)

4.1.4. Ignition System

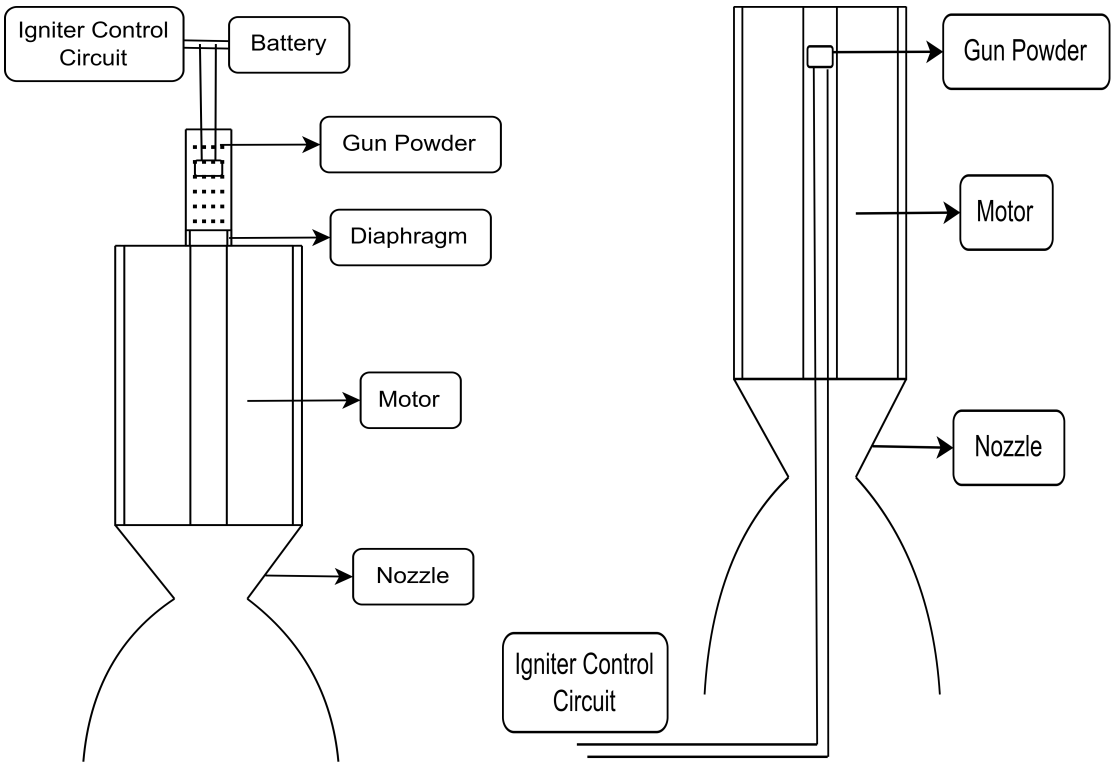

Figure 4.10: Type A (left) and Type B (right) Igniter

The rocket's motor required an ignition system to initiate combustion. The choice of ignition system was critical because the burning surface of the fuel significantly impacts motor performance, affecting thrust, impulse, burn time, and pressure. In our case, it was essential to ignite the entire surface of the core initially. There are two methods for igniting the core.

In the first type of igniter, labeled Type A, the igniter was positioned at the motor's top and contained a canister with a black powder charge. This black powder is ignited using a nichrome wire heated by a power source. The pressure resulting from the black powder explosion then initiated the fuel combustion. The onboard computer can control the entire ignition system in this case.

In the second type of igniter, referred to as Type B, the igniter was inserted through the nozzle from the bottom. A small packet of black powder, along with a nichrome wire, was placed at the top of the motor through the nozzle. The gunpowder ignited through the nichrome wire, powered by the ground station. Consequently, the pressure generated by the burning black powder expelled the ignition system from the motor and

ignited the fuel.

Both types of igniters were tested. Type A proved more effective than Type B, as it doesn't impede the flow during combustion. However, Type A faced gas leakage issues due to the necessity of connecting the nichrome through the engine block of the motor tube. On the other hand, Type B, despite obstructing the flow, was comparatively simpler. Additionally, leaving the ignition system on the ground reduces the rocket's weight during tests.

4.1.5. Static Test

A thrust stand was essential for conducting static thrust measurements on a motor. The static tests provide crucial data regarding propellant performance, thrust, burn time, total impulse, and specific impulse. This data allows for the evaluation of key parameters such as chamber pressure, characteristic velocity, and thrust coefficient.

In the earlier design of the thrust stand, a linkage mechanism was utilized to secure the booster against the load cell. As part of a project initiative, this linkage mechanism was replaced with linear bearings and a dedicated platform to support the motor.

(a) (b)

Figure 4.11: (a) CAD design of Linear Bearings (b) Thrust Stand

(a) (b)

Figure 4.12: Static Test

4.1.6. Ballistic Evaluation Motor

Ballistic Evaluation Motor (BEM) was used to evaluate the ballistic parameters such as burning rate, specific impulse, and thrust[11]. The setup for this motor is illustrated in the figure 4.13. The principle of this method is simple. End burning of surface area ensures constant throughout the burn time resulting in constant steady state pressure.

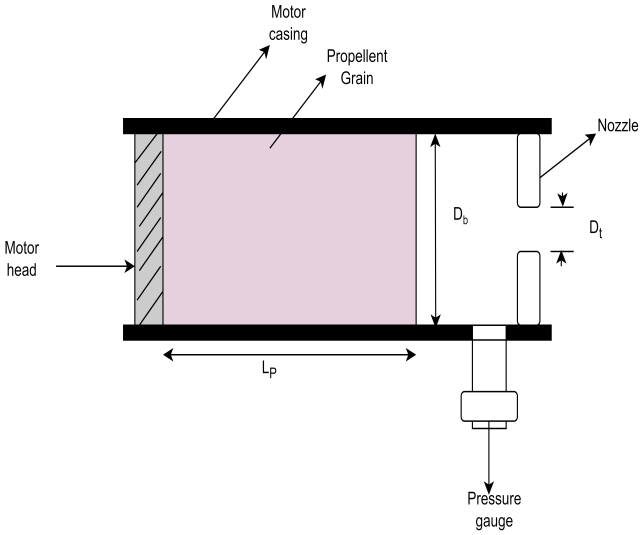

(a)

(b)

Figure 4.13: (a) Schematic representation of BEM Setup (b) BEM Setup

The steady-state chamber pressure is given as,

$$P_0 = c^*.\rho.r.K_n \tag{4.1}$$

and from the Saint Robert's law,

$$r = \alpha.P^n$$

where,
r is the burn rate.
K_n is the ratio of the burning surface (A_b) to the area of the throat (A_t). For the different diameters of the throat, Kn is different. Hence, the value of burn rate coefficient(α) and pressure coefficient(n) is obtained.
For the slow-burning propellant, the end burning grain configuration may not be effective to generate required chamber pressure or size of throat required is small. In this case, side burning with the slab grain can be used[8].

4.1.7. Pressure Chamber (Crawford Strand Burner)

Figure 4.14: Crawford Strand Burner

A strand burner is an apparatus designed for measuring the burn rate of solid propellants under elevated pressure conditions. In this experimental setup, a defined length of the propellant was carefully arranged within a chamber, subject to controlled pressure conditions. Two ends of the propellant strand were positioned in contact with thermocouples, allowing for the precise measurement of temperature at each end. The temperatures recorded by the thermocouples, along with corresponding time stamps, were crucial data points. The burn rate of the propellant was determined by analyzing the

time difference between the peak temperatures recorded at the two ends. This process was repeated at different chamber pressures. The resulting data burn time at defined pressure was used to calculate the burn rate coefficient (α) and pressure exponent (n).
The configuration comprised a steel tank with hemispherical ends, aimed at reducing bending stress within the chamber. A ball valve was installed at one end to regulate chamber pressure, connected to the chamber via a GI pipe union coupler. Gas filling from the compressor to the chamber was facilitated by a Quick Release Coupler Connector, a pneumatic fittings air line hose compressor connector.
Burn duration was determined using two sets of K-type thermocouples (chromel-alumel) due to their excellent linearity of the electromotive force (emf) in relation to the measurement temperature. These thermocouples were capable of measuring temperatures up to 1260°C, encased in metal shield braiding and equipped with an M6 screw-on stainless steel probe. Each thermocouple had a wire length of 500 cm, and they were positioned 10 cm apart from each other inside chamber. The burn rate of the propellant strands at elevated applied pressure was determined by dividing the distance between the thermocouples by $t_2 - t_1$ (as shown in figure 4.15). Time t_1 and t_2 corresponds to the time at which temperature begins to rise in thermocouple 1 and peak temperature indicated by thermocouple 2 respectively.

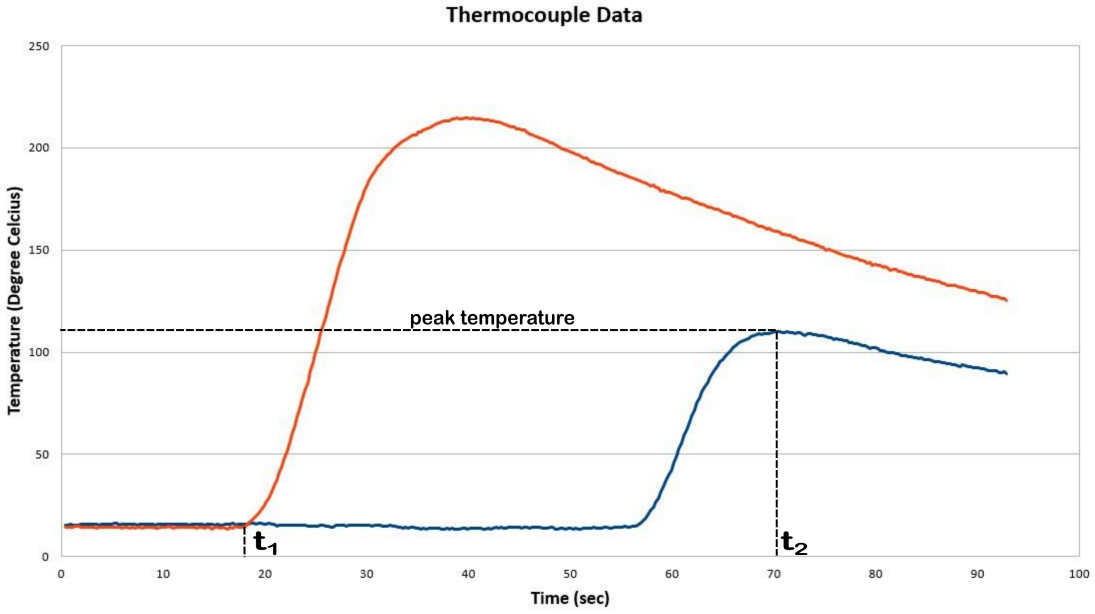

Figure 4.15: Plot of Thermocouple Data (Temperature vs Time

4.2. Aerodynamics

The aerodynamics of a rocket play a pivotal role in its performance and trajectory through the atmosphere. In the context of our sounding rocket designed for atmospheric studies, the aerodynamic considerations were paramount for ensuring stability, control, and optimal performance during ascent and descent.

4.2.1. Nosecone

The nose cone's form is essential in reducing aerodynamic drag as the rocket ascends. Various nose cone shapes, including conical, ogive, or parabolic, influence the airflow around the rocket, diminishing resistance and enhancing overall stability. Given that the parabolic shape minimizes drag, it was preferred for its aerodynamic efficiency.

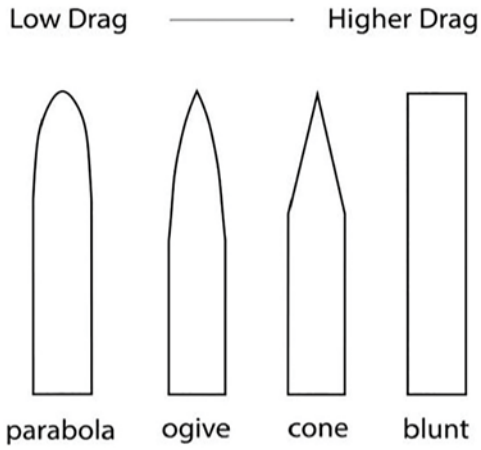

Figure 4.16: Drag on different shapes of Nosecone
[3]

4.2.2. Fins

Fins are integral to a rocket's aerodynamics, serving as crucial elements intended to enhance stability, control, and overall flight efficiency. They contribute to stability by generating aerodynamic forces that resist deviations from the intended flight path, ensuring a straight trajectory and preventing tumbling or spinning.
The positioning of fins also impacts the rocket's center of pressure (CP), the point where the sum of aerodynamic forces is considered to act. Well-placed fins guarantee that the CP is located behind the rocket's center of gravity (CG), enhancing stability. Fins create both drag and lift forces, with drag aiding in stabilization and lift counteracting the rocket's weight. The lift direction typically aligns perpendicular to the rocket's longitu-

dinal axis.

The dimensions, shape, and orientation of fins significantly influence aerodynamic performance. Larger fins generally offer increased stability but may also elevate drag. Different fin shapes, such as trapezoidal, elliptical or delta, exhibit distinct aerodynamic characteristics. Fins can influence the angle of attack (AoA), defined as the angle between the rocket's longitudinal axis and the oncoming airflow. Maintaining an appropriate AoA is crucial to prevent instability. Ensuring the proper attachment of fins to the rocket body is essential. The attachment method, including the number and placement of fins, plays a pivotal role in determining overall aerodynamic performance.

4.3. Airframe System

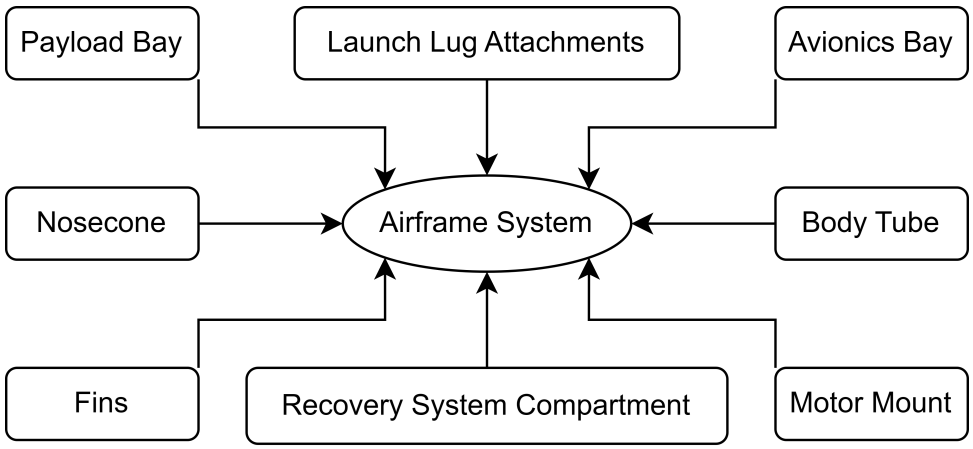

Figure 4.17: Components of Airframe System

4.3.1. Body Tube Fabrication

During the creation of the sounding rocket, the pivotal aspect of the process involved the fabrication of the body tube. This component played a crucial role as it accommodated nearly all rocket elements, shielding them from external environmental factors. The body tube enclosed the flight computer, ejection bay, payload components, motor/engine, and recovery systems, while also serving as the attachment point for fins, nosecone, and launch lugs. To meet specific criteria, the body tube or fuselage must possess qualities such as rigidity (resistance to deformation upon impact), ease of modification for component assembly, compatibility for attaching various tubes, and, importantly, lightweight construction with uniform thickness to prevent undue weight increase.

Considering these requirements and constraints, the body tube was constructed using a glass fiber composite. The fabrication process involved utilizing a mixture of resin and hardener combined with fiber cloth and glass fiber. The resulting density of the developed fiber composite was 0.95 gm/cm^3. Another potential material option for the body tube was PVC pipe, which has a density of 1.4 gm/cm^3. However, manual structural testing revealed that the PVC pipe suffered damage upon impact. As a result, the choice was made to use the glass fiber composite for the actual body tube, meeting the specified criteria for the sounding rocket's construction. The step-wise method of fabrication is mentioned below:

Step 1: Define Dimensions: Specify the size (diameter and length) of the body tube.

Step 2: Establish Fabrication Setup: Create the necessary arrangement for constructing the body.

Step 3: Choose/Create Mold: Select or create a mold for layering the fiber.

Step 4: Prepare Setup with Filament Winding Method: Set up the apparatus with the filament winding method for composite fiber development.

Step 5: Utilize Butter Paper: Apply butter paper in the initial layer to prevent the composite from sticking to the mold.

Step 6: Place Fiber Cloth Layer: Add a layer of fiber cloth.

Step 7: Apply Resin Mixture: Paint a prepared resin mixture over the cloth to wet it, removing excess resin.

Step 8: Roll Glass Fiber Layer: Roll a layer of glass fiber after completing the first layer, similar to step 7. This combines the flexibility of the cloth with the strength and rigidity of the glass fiber.

Step 9: Add Final Fiber Cloth Layer: Place a final layer of fiber cloth and paint a finishing layer of resin.

Step 10: Allow Model to Dry: Leave the model to dry for 24 hours under standard room conditions. And remove the model from the mold.

Figure 4.18: Final Model of the Body Tube

Step 11: Conduct Manual Structural Drop Test: Test the body tube through a manual structural drop test to ensure it can withstand impact.

4.3.2. Nosecone

The nose cone is an essential component within the airframe structure of a rocket, positioned at its forward-most part and designed to perform diverse functions related to aerodynamics, structural strength, and safeguarding the payload. The primary roles of the nose cone within the airframe structure include:

- Structural Support:
  The nose cone actively contributed to enhancing the overall structural strength of the rocket. It established a connection with the body tube or fuselage and imparts rigidity to the front end of the rocket. Considering structural aspects, the nose cone was manufactured using TPU.

- Payload Protection and Integration:
  The nose cone acted as a protective housing for the payload, encompassing components such as a microcontroller, sensors, battery, and various electronic elements. It served to shield the payload from the effects of aerodynamic forces, atmospheric conditions, and potential damage during the rocket's ascent.

- Attachment Point for Recovery System:
  Frequently serving as the attachment point for the recovery system, the nose cone hosted the deployment mechanism for parachutes or alternative recovery devices for the payload. This feature significantly contributed to ensuring the secure descent of the payload during the recovery process.

4.3.3. Motor Mount

Motor mounts play a crucial role in securing and supporting the rocket motor, providing structural stability, and ensuring the proper functioning of the propulsion system during flight. The attachment of the motor to the body tube and bulkhead involved the use of flanges, centering rings, and inner body tubes. To ensure reliability and flexibility, a method is adopted that allows the placement of the grain just before the test, preserving the fuel from the effects of humidity and the environment. Additionally, the motor mount served as the point of attachment for the fins and was designed to be compatible and adjustable, facilitating easy attachment to the body tube.

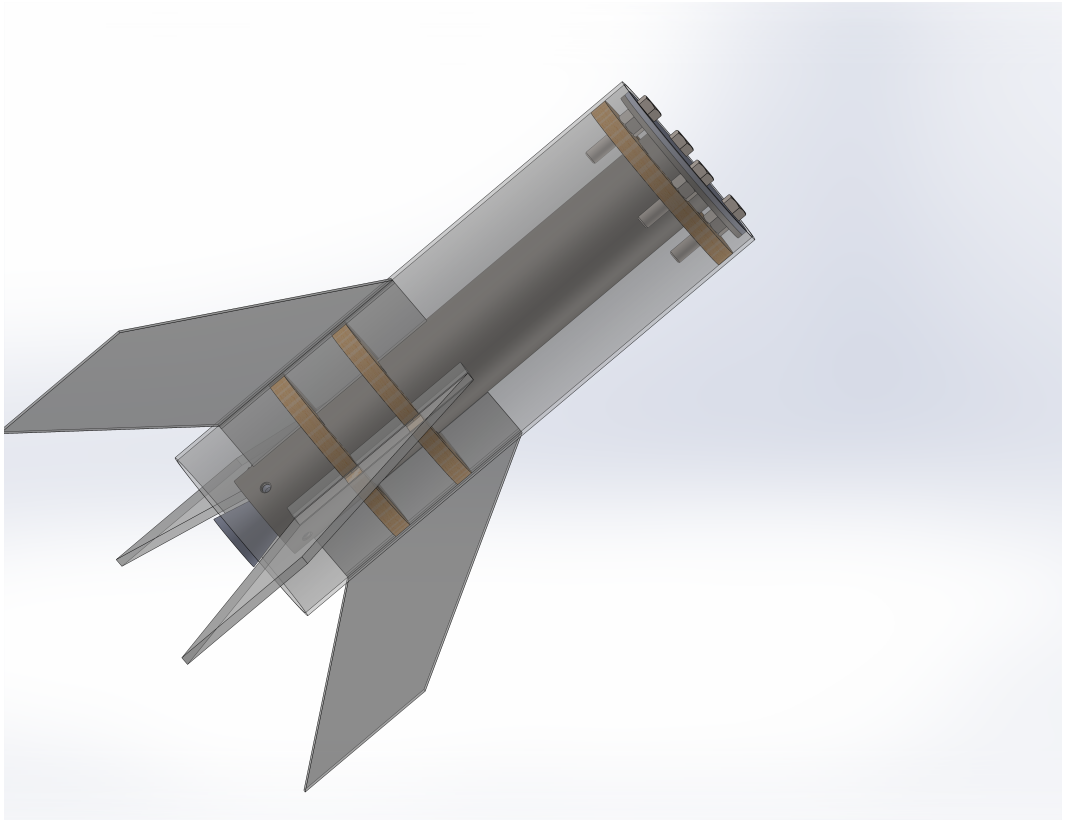

Figure 4.19: Motor Mount and Fins Assembly

4.3.4. Avionics Bay

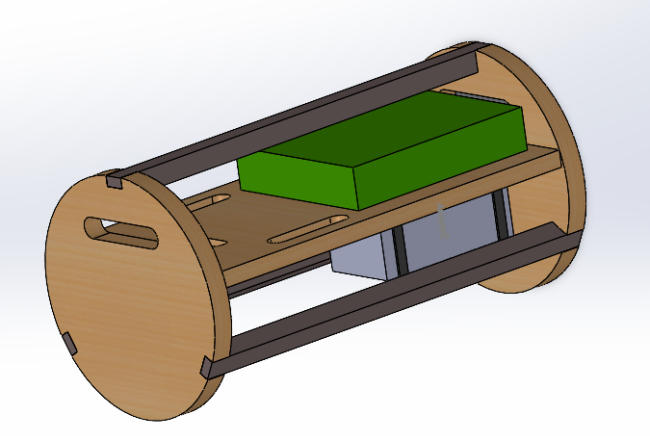

Figure 4.20: Avionics Compartment with Battery (bottom) and Electronics (top)

The avionics bay served as the enclosure for electronic elements, power distribution, and wiring. It was configured to include vents that facilitate the interconnection of wires, as illustrated in the figure, and to accommodate the attachment of electronic components. Within the avionics bay, the electronics were contained within a dedicated electronic box featuring vent holes. This design was particularly important for sensors like BMP 180, which need to sense the external ambient air. The avionics bay incorporated support pillars to ensure the stability of the electronics, preventing disarray in the event of an impact.

4.3.5. Payload Bay

The payload bay served as the enclosure for electronic elements which includes microcontroller and atmospheric data sensors. It was connected to the parachute and was released separately when the rocket reached its maximum altitude. The electronic components were enclosed within a dedicated electronic box featuring access holes through which sensors are in contact with the air to obtain atmospheric data. Enclosed within the body's nosecone, the payload bay comprised three distinct sections. At the base, there was a compartment housing a microcontroller and an SD card module. In the middle section, a compartment accommodated GPS and GSM modules. The uppermost section was dedicated to atmospheric data sensors. The atmospheric data sensors were placed in the uppermost section to ensure continuous contact with the surrounding atmosphere while collecting data during its descent.

4.3.6. Fins

Fins play a crucial role in the aerodynamics and stability of a rocket, as they were positioned externally to the body tube and subjected to aerodynamic forces such as lift and drag. The selection of their shape and dimensions was based on simulations conducted using OpenRocket software. Should a single fin detach or sustain damage, it can result in significant instability for the rocket. Therefore, careful attention to the design and attachment of the fins was essential. Materials like acrylic sheets was considered based on requirements, ease of fabrication, and attachment.

The placement of the fins was another critical factor. To counteract the effects of lift on the fins, they were positioned parallel to the body tube. Fins were integrated into the tube to form a single component, and this assembly was then inserted into the body tube. This approach helped eliminate assembly errors, particularly in areas with cutouts in the body tube.

4.3.7. Recovery System Compartment

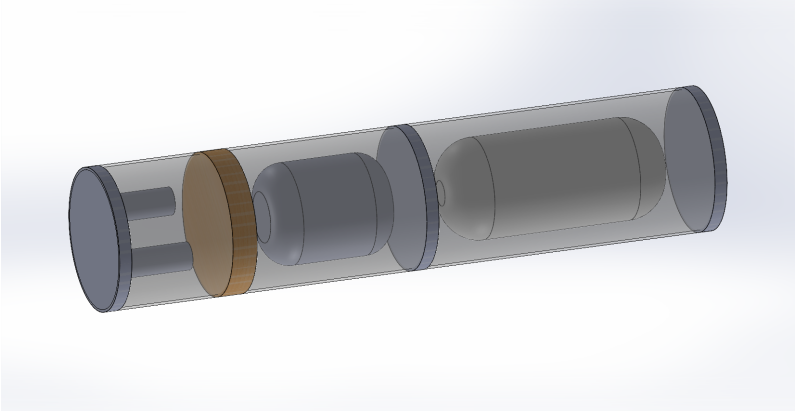

Figure 4.21: Recovery System Compartment with Black Powder Canister, Drogue Parachute, and Main Parachute (from left to right)

The recovery compartment comprised three distinct sections: the ejection charge compartment, the drogue compartment, and the main parachute compartment. These segments were housed within separate tubes, allowing for individual assembly and subsequent integration into the primary airframe. The ejection compartment, a sealed and pressurized tube, utilized the pressure generated by a black powder charge to facilitate the separation between the lower motor section and the upper airframe. This design ensured modularity and ease of integration for the recovery system within the overall structure of the designed vehicle.

4.4. Launch Stand

4.4.1. Introduction

An above-ground structure used for the vertical launch of a rocket, missile or spacecraft is called a launch stand. Launch stand can refer to the entire complex (launch complex) or just the primary launch platform (mobile launcher platform).

A simple model of launch stand that can support the rocket and guide it during the initial phase of its flight was designed and fabricated.

4.4.2. Geometry

The launch stand of height 300 cm that contained four vertical mild steel section of 1 by 1 inch and a base plate of normal plywood of thickness around 20mm was made in order to support our rocket of height 1.8-2 m.

Figure 4.22: Rocket body loaded in Launch Stand

4.5. Avionics and Payload

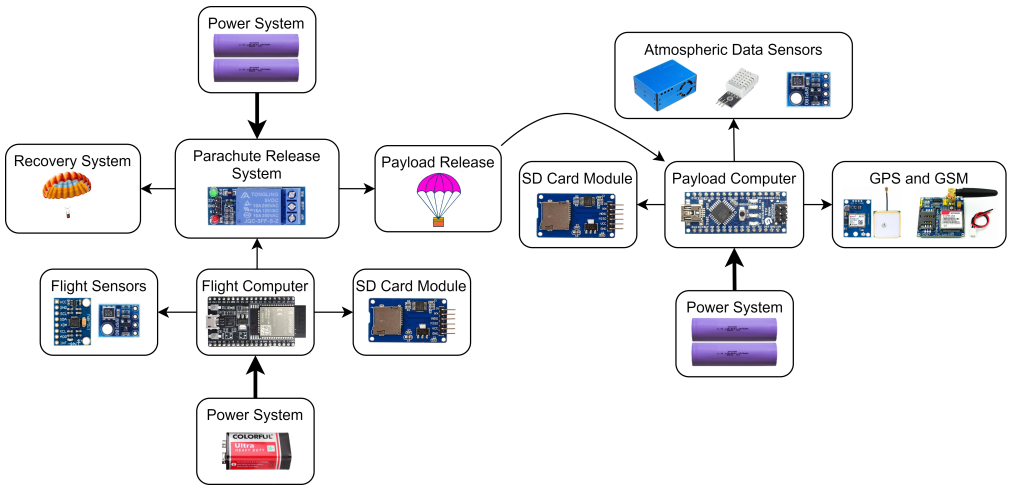

Figure 4.23: Components of Payload and Avionics System

4.5.1. Electronic Components

1. **Flight Computer :** The flight computer was utilized in order to regulate the ignition system, activate the recovery mechanism, and release the payload during launch. The flight sensors were included which gathers the flight data. The payload also consisted of flight computer. It contained flight sensors to gather flight data and atmospheric data. The battery was used as a power source for both these flight computers. The obtained data was post-processed to obtain flight information and atmospheric data.
   The flight computer consisted of a microcontroller (ESP32 and Arduino Nano), accelerometer (MPU6050), altimeter (BMP180), and SD Card Module. The microcontroller, sensors, and modules were connected to the battery through a voltage regulator (LM2596 DC-DC Buck Converter Step Down Module).

2. **Flight Sensors :** MPU6050 was used as an accelerometer. This sensor gives values of linear acceleration and angular acceleration in the x, y, and z axes. This value was post-processed to determine the trajectory of the rocket body. BMP180 was used as an altimeter. This sensor gives values of the altitude of the rocket body based on differences in atmospheric pressure concerning altitude. This altitude value was used as a logic circuit for the release of the parachute at the maximum height.

3. **Data Storage :** SD Card Module was used for flight data storage. The data from sensors were stored in an SD card. The data obtained then were post-processed

to get the required information on the flight path.

4. **Power Systems :** The microcontroller was powered using a 2 3.7 Volt 2-shell lithium-ion battery through a voltage regulator. LM2596 DC-DC Buck Converter Step Down Module was used as a voltage regulator to step down the voltage obtained from the lithium-ion battery. The voltage was stepped down to 5 Volt to power the microcontroller. The pyro technique was used in the recovery deployment system. An additional battery was needed for igniter.

5. **Recovery Deployment System :** The release of the parachute through the pyro technique was triggered through the relay. The relay was triggered using a microcontroller using the data obtained from the altimeter. The relay was triggered as soon as the altitude of the rocket body starts decreasing from its maximum altitude. Payload was deployed initially and then the recovery system for the body was deployed.

6. **Atmospheric Data Sensors :** The payload of the system consisted of a microcontroller with atmospheric data sensors. The data sensors for the atmospheric data collection were PM (Particulate Matter) sensor (PMS5003T) to measure particulate matter in the atmosphere, DHT22 sensor to measure temperature and humidity and BMP180 to measure atmospheric pressure. GPS module was also included in the payload to obtain location data. GSM module was included which acted as a telemetry that sends location data during flight.

4.5.2. Avionics System

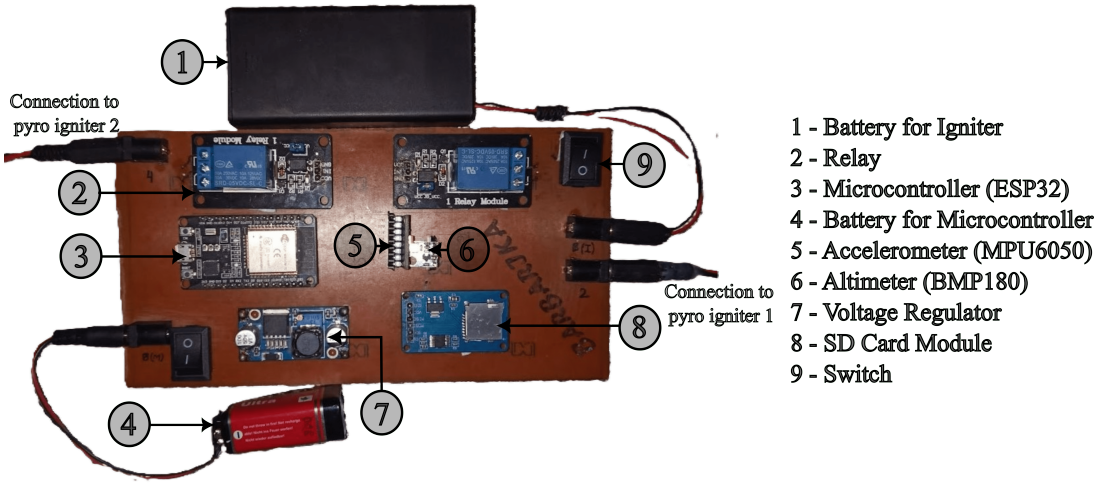

Figure 4.24: Avionics System

In the avionics system, ESP32 was used as a microcontroller, BMP180 as an altimeter, MPU6050 as an accelerometer, and relay to activate the pyro technique to release the parachute.

4.5.3. Payload System

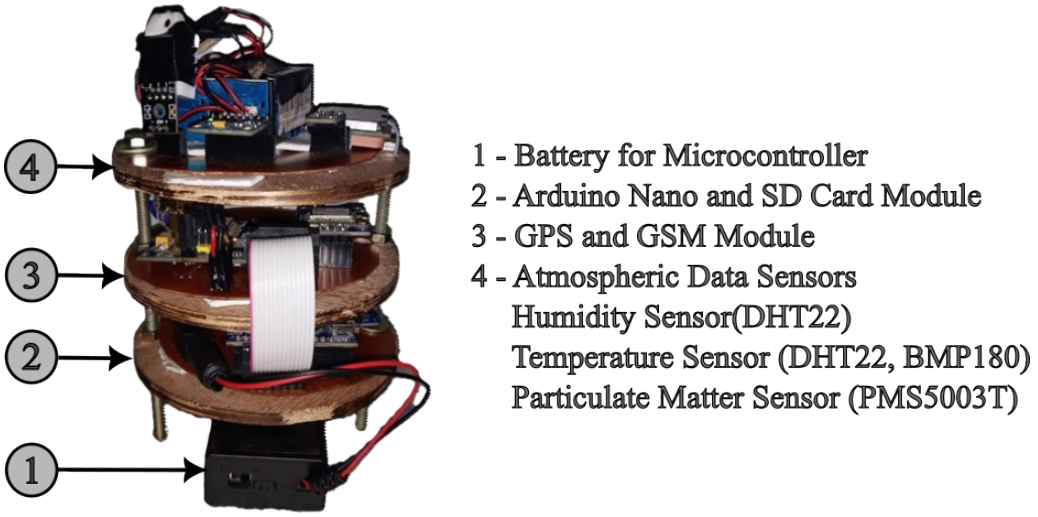

Figure 4.25: Payload System

In payload, Arduino Nano was used as a microcontroller, BMP180 as a pressure sensor, PMS5003T as particulate matter (PM) sensor, DHT22 sensor as humidity and temperature sensor, GPS module to obtain the location of payload, GSM SIM 900 to send location data.

4.5.4. PCB Fabrication

The PCB fabrication was done in a single-side copper layer printed circuit board.

Step 1: PCB Design: PCB was designed in software (KiCAD) based on required electronics and dimensions.

Step 2: Design Print: The mirrored PCB design was printed on special transfer paper using a laser printer.

Step 3: Copper Board Preparation: The copper-clad board was cleaned with sandpaper to make it free from oxidation or contamination.

Step 4: Design Transfer: The printed side of the transfer paper was aligned to the copper board. A laminator was used to apply even pressure and heat which transfers the toner onto the copper board.

Step 5: Cooling and Peeling: The board was allowed to cool down and the transfer paper was gently peeled off. The toner stuck to the copper board showing your circuit design.

Step 6: Etching: The board was immersed into the solution of HCl and H_2O_2 (ratio = 1:3). The exposed copper was dissolved, leaving only the traces protected by the toner.

Step 7: Cleaning and Inspection: After etching, the toner was removed using acetone. The board was cleaned thoroughly. The board was inspected thoroughly.

Step 8: Drilling and Finishing: The holes for component leads and mounting were drilled.

Step 9: Soldering Components: The components were soldered using soldering wires using soldering iron.

4.6. Recovery System

The recovery system consisted of a drogue and a main parachute. The main parachute was hemispherical and was manufactured with lightweight taffeta fabrics. A thin braided nylon cord was used for the suspension lines.
Small parachutes using paper was initially created to confirm their shape and design. Following that, a miniature fabric parachute using nylon was made to confirm the viability of the manufacturing process. The main parachute was manufactured based on the reference of these prototypes.
The assembly was designed in such a way as to ensure the ejection of parachutes by limiting the amount of pressurization volume using the recovery tube. The use of a recovery tube also allowed quick and more efficient integration into the rocket. The concept of using a recovery tube was developed after the first test of the recovery system in which the parachute tangled with the pins of the main body. The separation of the rocket body was triggered by the black powder charge. In our case, because of the low apogee, a single triggering mechanism was used, and the main parachute was completely pulled by the drogue parachute.
The square canopy parachute was used for the design. These parachutes were easy to manufacture and had high drag coefficients ranging from 0.75 to 0.8[5].

4.6.1. Design Decisions

1. **Separation Method:** The black powder charge canister was successfully tested for triggering the deployment system. Even though, there was inherent variability of performance of black powder, especially at high altitudes (because of low pressures) [19], decision was solely based upon the fact that the apogee was below one kilometer and there were no significant pressure changes. In the alternative, a CO_2 canister-based deployment system was also studied but later it was dropped as it proved to be costly.
   The amount of black powder charge required for the separation is given as,

   Charge needed for separation = (Inner Diameter of Body Tube)^2 x (Length of Body Tube) x 0.006 [20]

2. **Self-contained system:** Rather than directly inserting the parachute in the body frame, an interference-fit inner tube recovery bay system was adopted. The recovery was packed and wired independently from the main airframe. This solved the problem of tangling of suspension lines with the main airframe. The fully assembled system was slid into the airframe, which eased our assembly process.

4.6.2. Sizing

A MATLAB program was constructed to size the main parachute based on "The Parachute Manual: A Technical Treatise on Aerodynamic Decelerators" by Dan Poynter (1984)[21]. The main parachute had an area of 2.94 m^2 and was designed to slow down the 8 kg rocket to the speed of 8 m/s. The calculations were done for 300m altitude; assuming the ground level for the launch site. The decent rate did not account for the drag caused by the rocket, which can be substantial. The drag coefficient of 0.7 was used as taffeta fabric was selected as material for parachute.
The drogue terminal velocity window was set to be between 20 and 25 m/s [5] to maximize the falling rate without incurring critical damage in the unfortunate scenario of the failed deployment system. The design of the drogue parachute was based on the weight of the main parachute system.

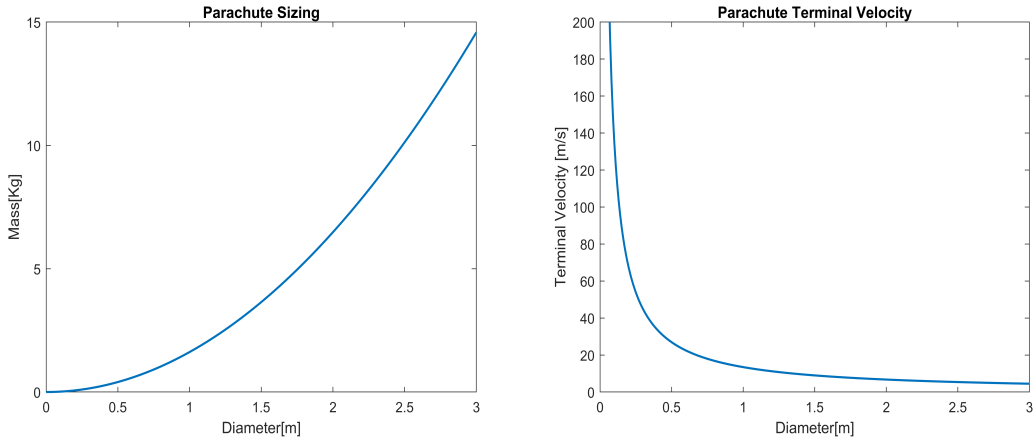

(a) (b)

Figure 4.26: (a) Parachute Sizing (b) Terminal Velocity vs Diameter

4.6.3. Configuration

The lengths of the shock cords were determined experimentally. They were determined to minimize the likelihood of the separated airframe halves colliding. They were also sufficiently long to decelerate upon separation so that the airframe sections did not rebound into each other when they hit the end of the cord.

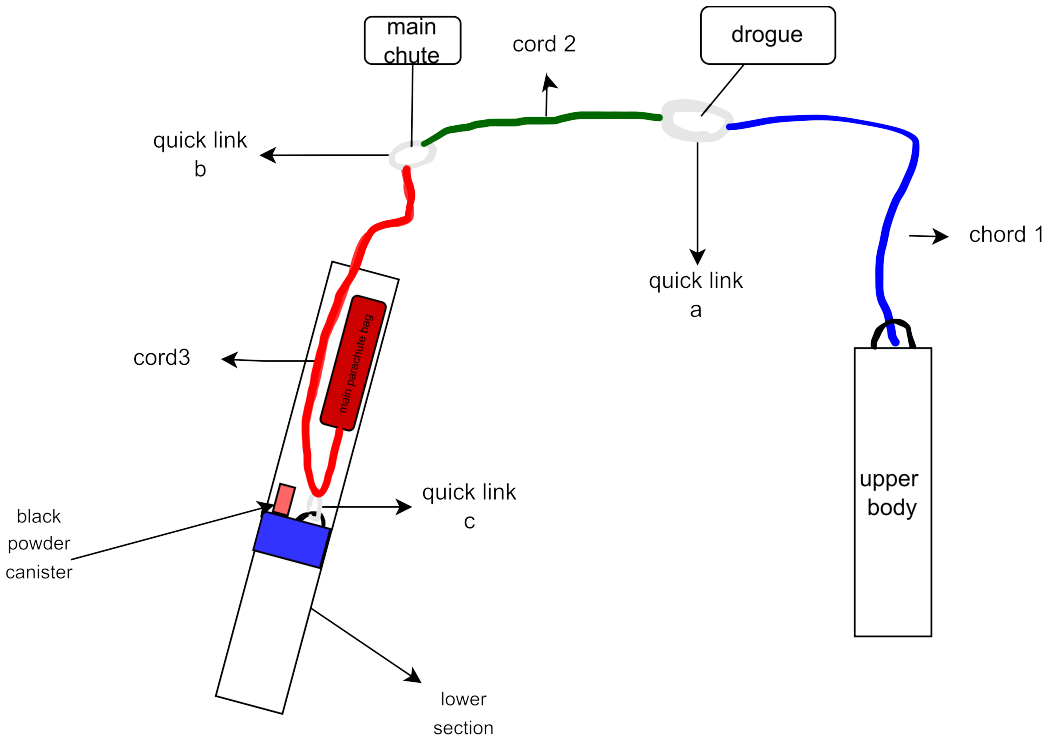

Figure 4.27: Schematic Representation of Recovery System

4.6.4. Fabrication and Testing

The parachutes were crafted using taffeta fabrics. Initially, the parachute for the payload was fabricated, checking the feasibility of the manufacturing process. Deployment of the parachute was also tested, achieving the desired inflation and drag. The drag coefficient of 0.68 was calculated. Subsequently, the drogue and main parachutes were fabricated. For visibility during deployment in flight, the drogue and main parachutes were made from contrasting colors.

(a)

(b)

Figure 4.28: (a) Parachute deployment test (b) Main parachute

The joints were seam-stitched to ensure the integrity of the connections. Suspension lines were made using drawstrings. During the ejection test, a small section of the canopy was damaged due to the gunpowder charge. This was patched and subjected to ground testing by running to ensure its effectiveness.

4.7. Body Assembly

The body was divided into three distinct parts: lower body, upper body and nosecone.

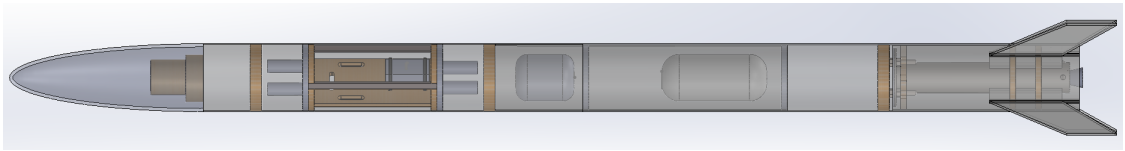

Figure 4.29: CAD Model of Rocket Body

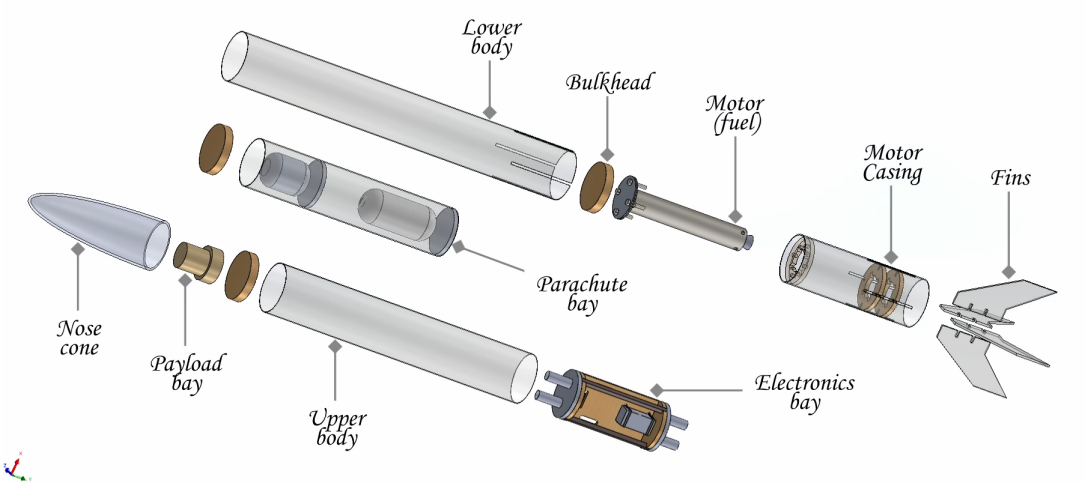

Figure 4.30: Exploded view of Rocket Body

Figure 4.31: Fabricated Full Scale Model of Phase I

4.7.1. Phase I

The total length of body was 186 cm and total mass of body was 6458 gm. The diameter of the body was 11.6 cm. The lower body consisted of a motor, fuel, fins and parachute bay. The motor was inserted into motor casing and was inserted to the lower body. The bulkhead was kept above the motor which was attached to the lower body. Centering rings were present to support the motor. Fins were attached to the body using cutout in the lower body. The upper side of lower body consisted of parachute bay which was attached to the lower body. The upper body consisted of electronics bay and black power charge canister to separate the body during recovery. The nosecone was attached to upper body.

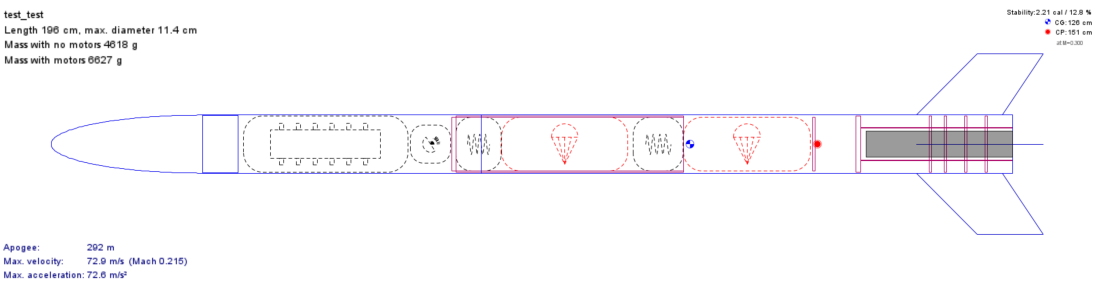

Figure 4.32: Full Scale OpenRocket Model of Phase I

4.7.2. Phase II

The total length of body was 212 cm and total mass of body was 9724 gm. The diameter of the body was 11.4 cm. The lower body consisted of a motor, fuel, fins and parachute bay. The motor was inserted into motor casing and was inserted to the lower body. The bulkhead was kept above the motor which was attached to the lower body. Centering rings were present to support the motor. Fins were attached to the body using cutout in the lower body. The upper side of lower body consisted of parachute bay which was attached to the lower body. The upper body consisted of electronics bay and two black power charge canister to eject the paylaod (nosecone) of the body and separate upper and lower body during recovery. Upper side of the upper body also consisted of the parachute for the nosecone. The nosecone was attached to the upper body which consisted of payload with atmospheric sensors.

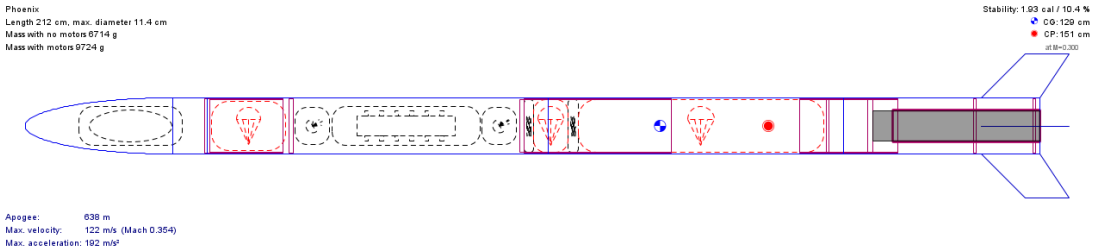

Figure 4.33: Full Scale OpenRocket Model of Phase II

CHAPTER 5: RESULTS AND DISCUSSIONS

5.1. Phase I

5.1.1. Static Thrust Tests

1. **Surface Inhibited Grain Configuration (December 21, 2023)**
   The static test of our propulsion system was accomplished. The mass of the motor (mixture of oxidizer and fuel) was 537 grams with a density of 1.8876 gm/cm^3. The four-grain motor was used where the length of each grain was 50 mm, having grain diameter and core diameter of 45 mm and 15 mm respectively.

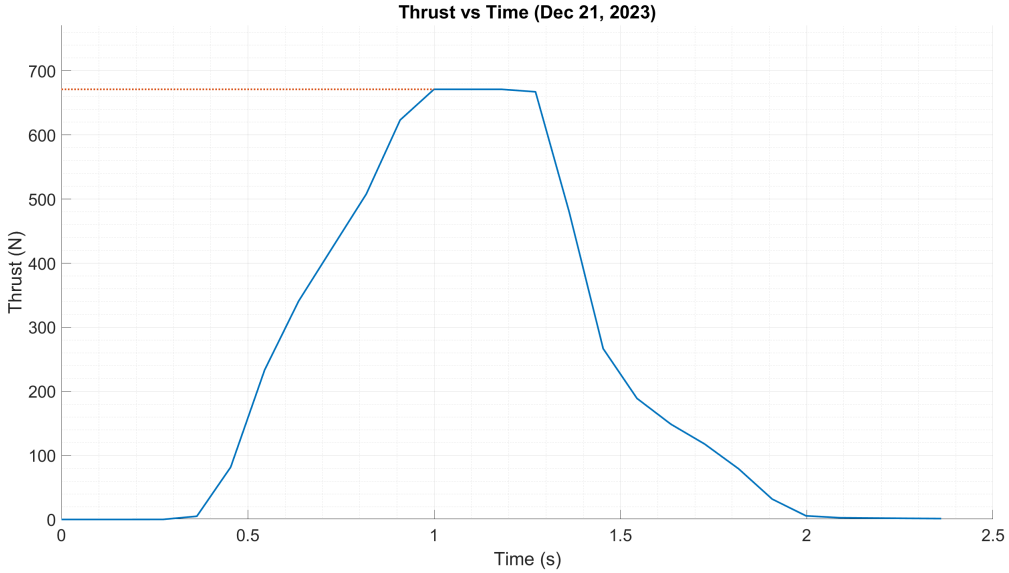

Figure 5.1: Thrust Curve (December 21, 2023)

The static test resulted in a burn time of 1.6 seconds with a peak thrust of 671 Newtons. The calculated values of total and specific impulse obtained were 580 Ns and 110 seconds.
The motor with the above specifications was incorporated into the OpenRocket design platform, the calculated peak altitude was 215 meters. The maximum acceleration and velocity were 106m/s^2 and 66.7m/s respectively.

2. **Surface Non-Inhibited Grain Configuration (February 1, 2024)**

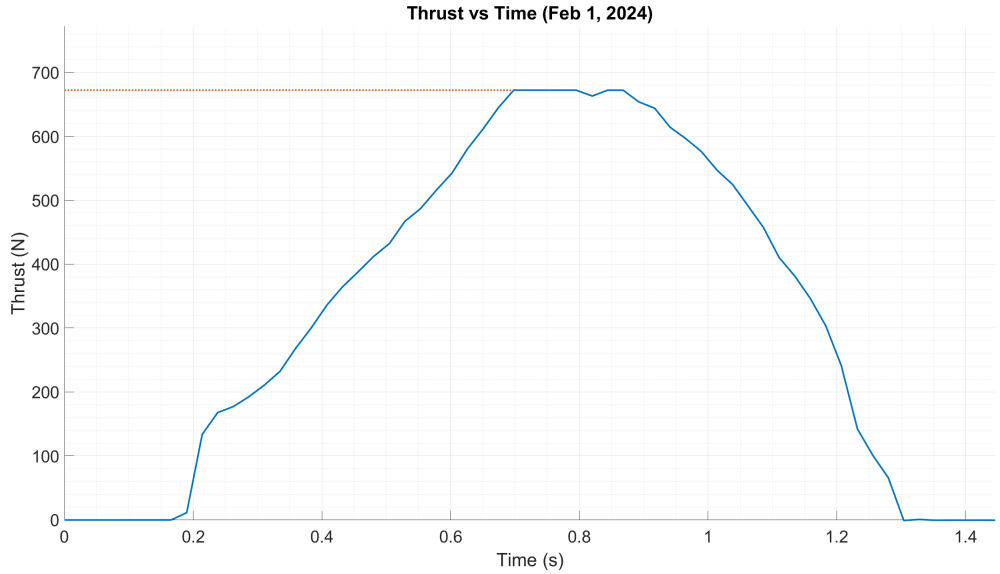

Figure 5.2: Thrust Curve (February 1, 2024)

The second static test, performed with a total mass of 472 grams, featured a grain lacking both inhibited surfaces, leading to a burn duration of 1.2 seconds and a peak thrust of 672 Newtons. The resulting total impulse was calculated as 478 Ns, with a specific impulse of 103 seconds.

3. **Surface Non-Inhibited Grain Configuration in Humid Environment (February 4, 2024)**

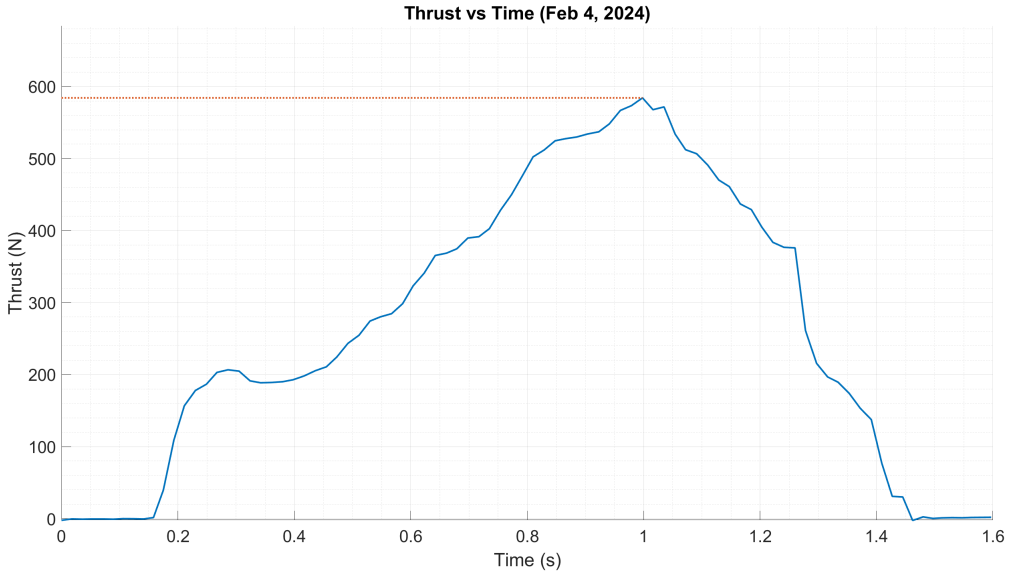

Figure 5.3: Thrust Curve (February 4, 2024)

The test was carried out using fuel that had been stored for two days and exposed

to a humid environment for several hours before testing. This led to a notable degradation in the performance of the fuel. Consequently, a burn time of 1.3 seconds was achieved, with a peak thrust of 584 Newtons.

4. **Surface Non-Inhibited Grain Configuration with Sealed Packaging (February 5, 2024)**
   The test was conducted with the fuel vacuumed and sealed, and precautions were taken to prevent exposure to the humid environment. As a result, the burn time lasted 1.24 seconds, reaching a peak thrust of 685 Newtons.

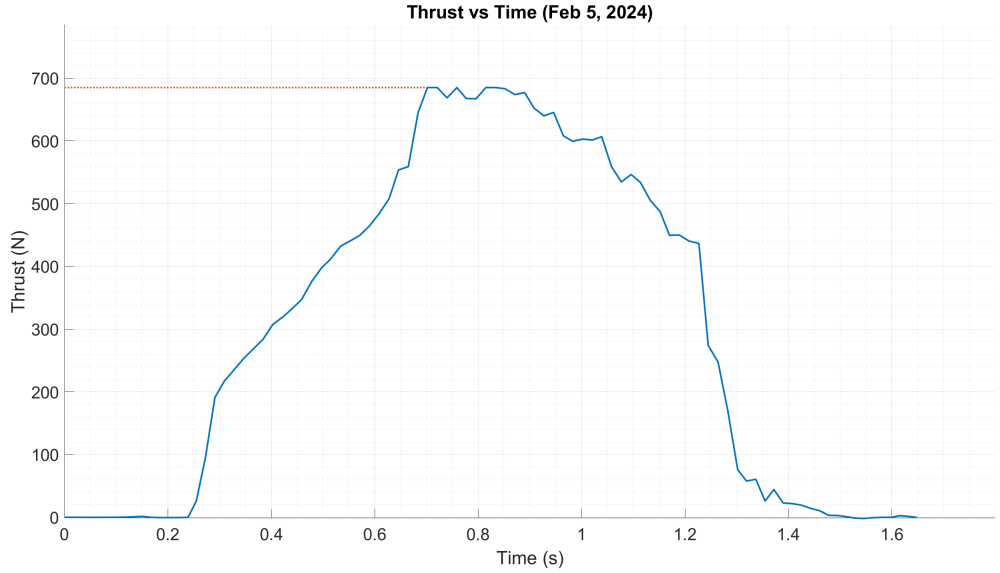

Figure 5.4: Thrust Curve (February 5, 2024)

Additional examination of the static test and the performance of the propellant reveals its high hygroscopic nature, making it susceptible to environmental factors such as humidity and temperature. Therefore, adequate airtight seals were necessary for prolonged storage. Surface inhibition significantly impacted both burn duration and the overall thrust curve.

5.1.2. Flight Test

The flight trial of Barbarika took place on February 6, 2024, aiming for an apogee of 250 meters. The setup comprised standard electronic components such as a flight computer, SD card storage, BMP 180, MPU 6050, GSM SIM900 Module, GPS Module, and power supply. However, the actual apogee achieved was 240 meters, following a vertical launch. This ensured the stability of the rocket. The deployment charge functioned as expected during this flight. Nonetheless, a malfunctioning cord led to a faulty

deployment of the parachute, resulting in the failure of the recovery system. Despite the crash, the structure remained intact, allowing for the full recovery of data and other components.

Figure 5.5: Flight Test of Barbarika (Phase I)

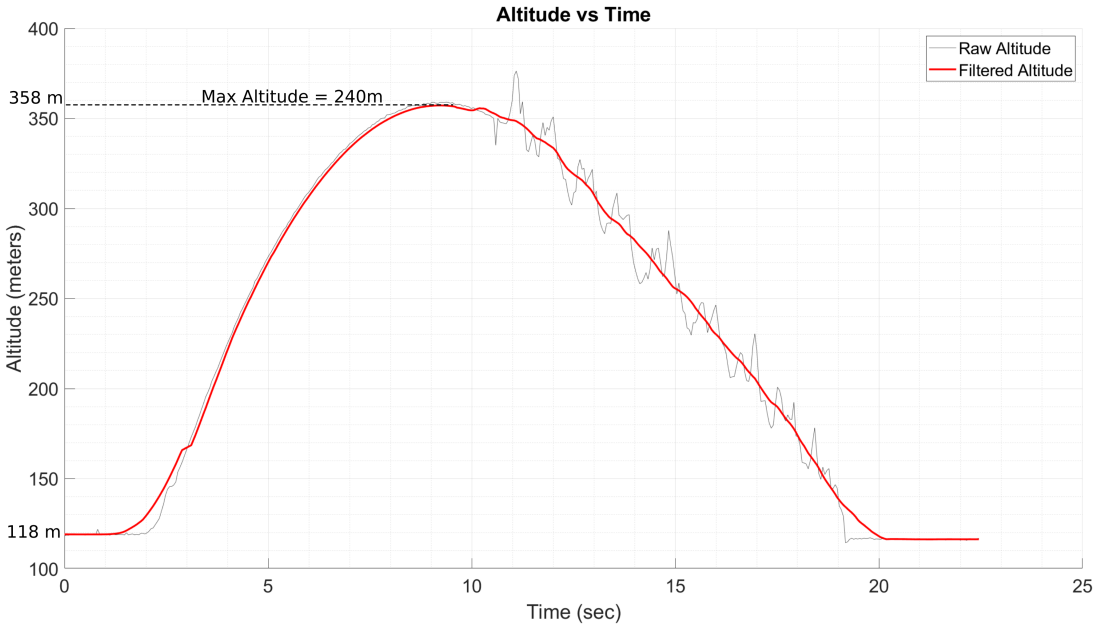

Figure 5.6: Altitude graph from the Phase I Flight Test

The graph displays altitude over time, showcasing both the original data and a filtered version obtained using the movmean function. The starting altitude of the test location

was 118 meters above sea level, with a peak altitude of 358 meters above sea level indicating the total height attained as 240 meters from the ground. The entire flight duration was 17.2 seconds, during which the rocket reached its maximum altitude of 7.2 seconds.

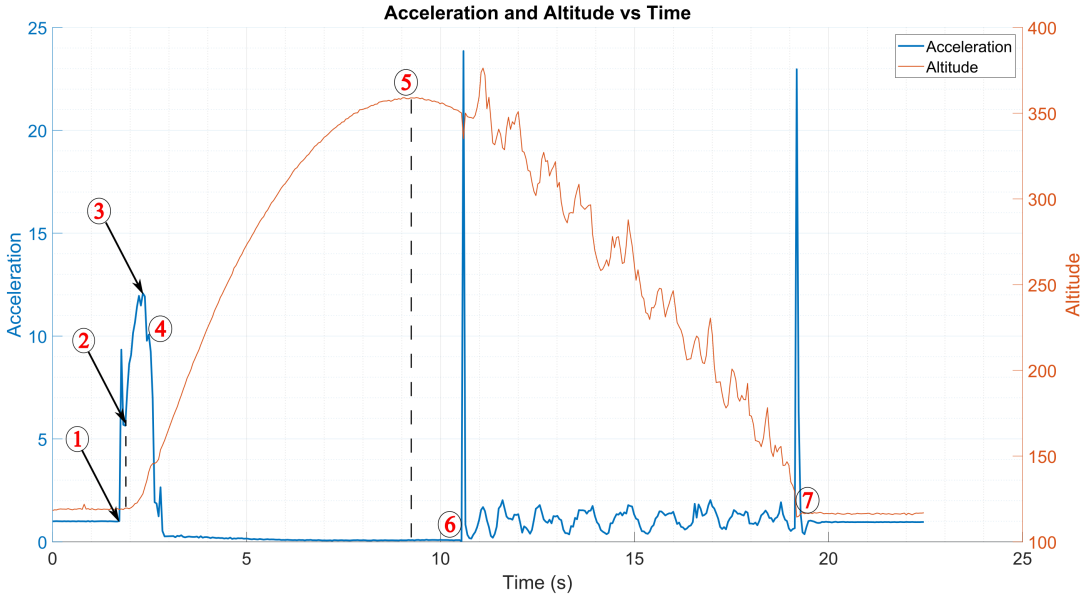

Figure 5.7: Graphical Representation of Phase I Flight Test

The graph represents the overall flight test. The acceleration data is compared with the altitude data to deduce the points. At point 1, ignition of the propellant was done, whereas at 2, the vehicle started to lift off, a sudden change in acceleration could also be seen. At point 3, the vehicle reached the maximum acceleration attained due to combustion, and there was a drop in acceleration. Point 4 signified the motor burnout. The vehicle reached the maximum altitude at point 5. After a 5-meter decrease in altitude, the ignition charge was triggered for the parachute deployment. It could be seen at point 6 and also signified by the sudden change in acceleration. After the body separation, the vehicle touched the ground at point 7.

5.2. Phase II

5.2.1. Static Thrust Tests

1. **Phase II Static Test with Non-Inhibited Grain Configuration (February 28, 2024)**
   The static test of the propulsion system for the Phase II flight test was conducted. The mass of the motor (mixture of oxidizer and fuel) was 1046 grams with a density of 1.8876 gm/cm^3. The five-grain motor was used where the length of each grain was 50 mm, having grain diameter and core diameter of 57 mm and 20 mm respectively.

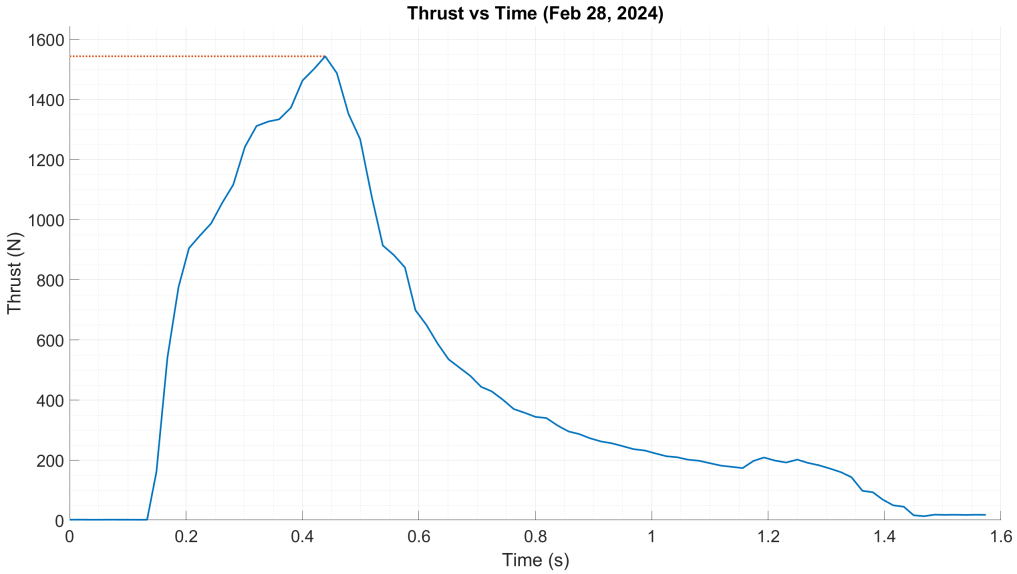

Figure 5.8: Thrust Curve (February 28, 2024)

The static test resulted in a burn time of 1.3 seconds with a peak thrust of 1543 Newtons. The calculated values of total and specific impulse obtained were 610 Ns and 59 seconds. The consequence was the failure of the bulkhead and an abrupt decrease in thrust caused by a drop in pressure.

2. **Phase II Static Test with Surface Inhibited Grain Configuration (March 4, 2024)**

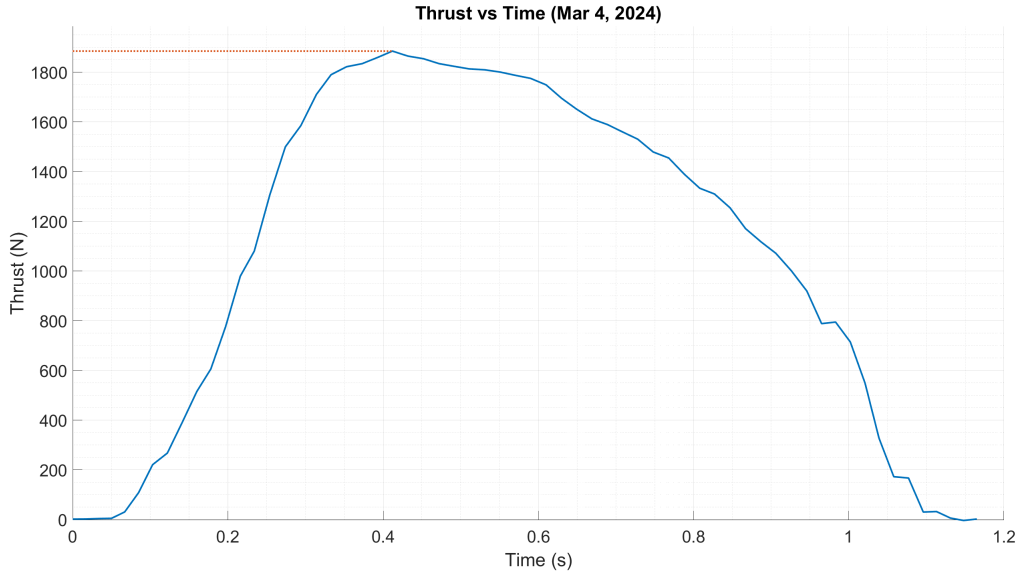

Figure 5.9: Thrust Curve (March 4, 2024)

The enhancements made to the bulkhead and grain configuration, incorporating surface-inhibited grain, yielded a maximum thrust of 1884 N with a burn time of 1.1 seconds during the static test. The calculated values for total impulse and specific impulse obtained from this test are 1237 Ns and 119 seconds, respectively.

5.2.2. Flight Test

The motor with a maximum thrust of 1884 N was selected for the Phase II flight test. Upon integrating this motor into the OpenRocket software, with a total weight of 9724 grams, it indicated an apogee of 638 meters and a stability of 1.93 calibers. Conducted on March 8, 2024, the test flight encountered failure due to nozzle detachment from the motor, resulting in a lift-off height of only 20 meters.

Subsequently, the motor initially designated for the Phase I flight test was repurposed to evaluate the deployment systems. The second flight trial, held on March 9, 2024, targeted an apogee of 170 meters. Equipped with avionics and a payload system, the actual apogee achieved was 114 meters, affected by wind velocity during the vertical launch. Despite this, the rocket demonstrated stability. During this flight, the deployment charge functioned as intended, facilitating both payload deployment and recovery system activation. The test experienced partial success due to insufficient altitude, preventing the parachutes from fully inflating and reaching terminal velocity.

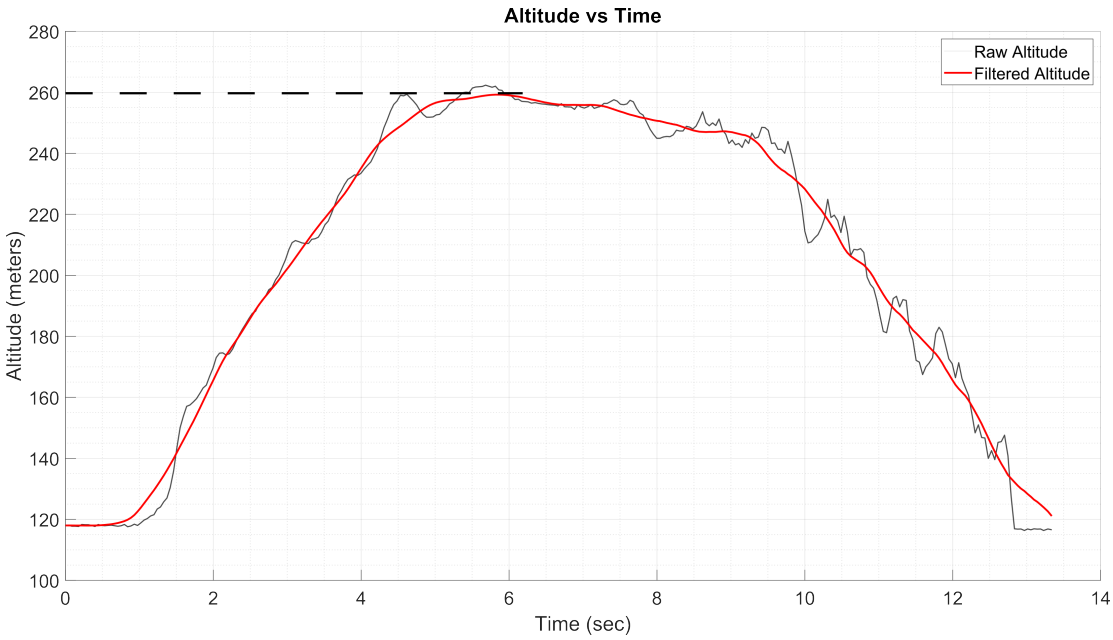

Figure 5.10: Altitude graph from the Phase II Flight Test

The graph displays altitude over time, showcasing both the original data and a filtered version obtained using the movmean function. The starting altitude of the test location was 118 meters above sea level, with a peak altitude of 262 meters from sea level with a total height of 144 meters from the ground. The entire flight duration lasted 12 seconds, during which the rocket reached its maximum altitude in 3.5 seconds.

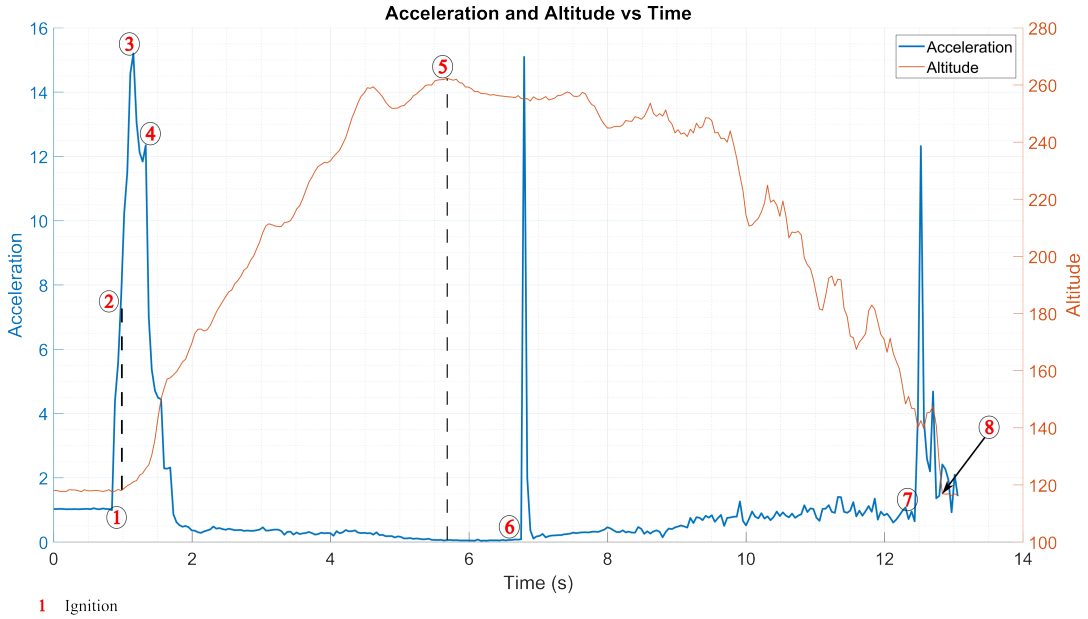

1 Ignition
2 Lift-off
3 Max Acceleration
4 Motor Burn-out
5 Max Apogee
6 Payload Deployment
7 Ejection Charge
8 Touchdown

Figure 5.11: Graphical Representation of Phase II Flight Test

The graph represents the overall Phase II flight test. The acceleration data is compared with the altitude data to deduce the points. At point 1, ignition of the propellant was done, whereas at 2, the vehicle started to lift off, a sudden change in acceleration could also be seen. At point 3, the vehicle reached the maximum acceleration attained due to combustion, and there was a drop in acceleration. Point 4 signified the motor burnout. The vehicle reached the maximum altitude at point 5. After a 5-meter decrease in altitude, the ignition charge was triggered for the payload deployment. It could be seen at point 6 and also signified by the sudden change in acceleration. The body separated for recovery parachute deployment after 5 seconds at point 7. After the body separation, the vehicle touched the ground at point 8.

5.2.3. Atmospheric Data

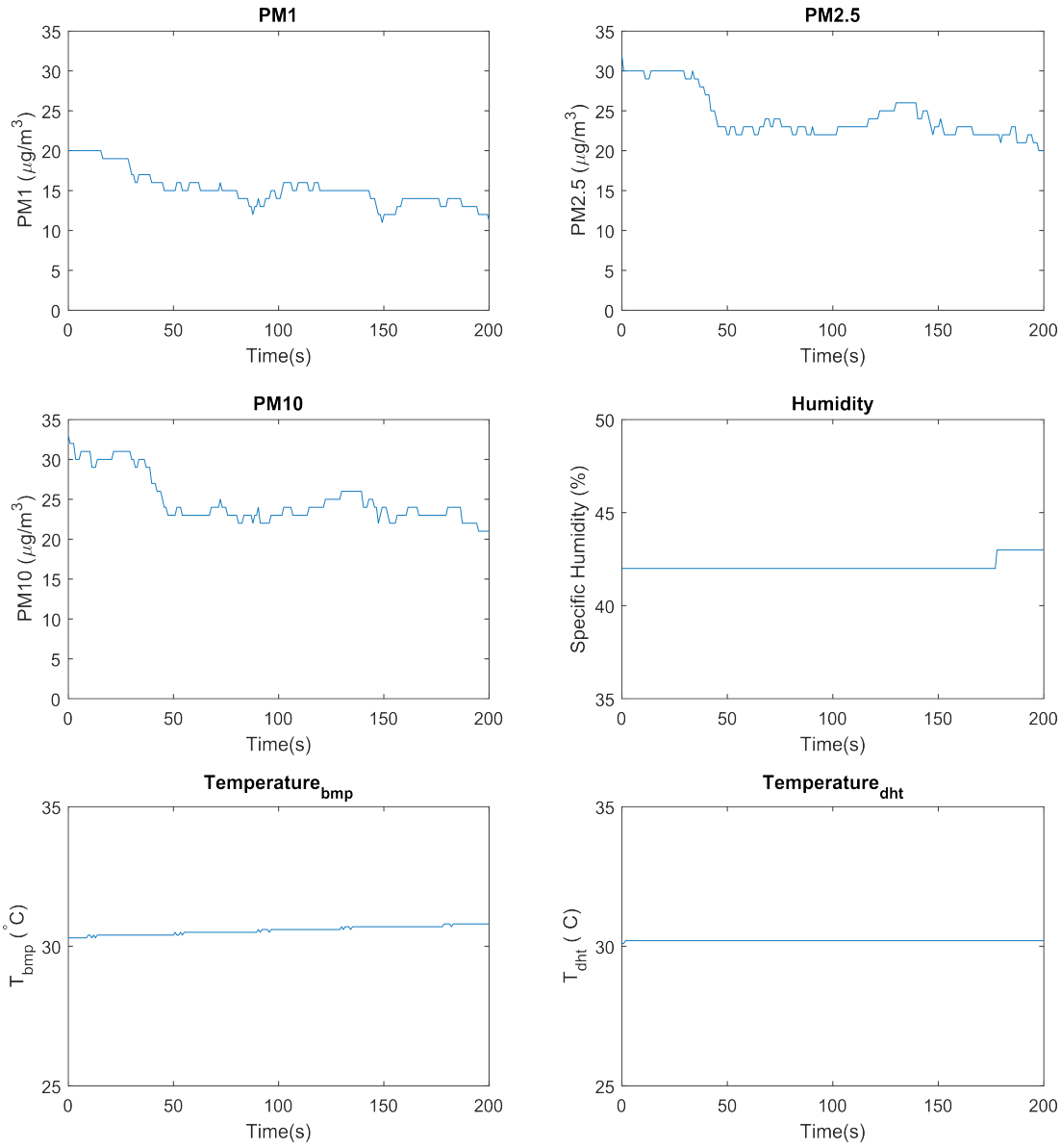

Figure 5.12: Atmospheric Data from Phase II Flight Test

The payload was equipped with PM sensors, humidity, and temperature sensors. Despite their capabilities, the low sampling rates of 1 Hz from the sensors and constrained flight duration rendered them incapable of providing the required measurements. Upon deployment at maximum altitude, the payload descended to the ground over a span of 8 seconds. However, it failed to achieve terminal velocity due to insufficient height above ground level for data collection purposes.

5.3. Problems Faced

- An issue was encountered with the burn rate of the propellant. This problem arose due to impurities present in the oxidizer (KNO_3) obtained from the supplier.
- In the Crawford Strand Burner setup for the pressure chamber test, the thermocouples were unreliable and provided inconsistent data. The Ballistic Evaluation Motor (BEM) method was simple and the initial test gave promising results.
- While working on the rocket's electronics, an issue with power distribution between the igniters triggering the black powder charge for separation and the microcontroller was encountered.
- The significant challenge during our motor test for the phase-II flight was pressure leakage from the chamber at the attachment point of the chamber and engine block.
- In some instances, the materials with the desired characteristics were either expensive or simply unavailable in the market.

5.4. Limitations

- The trajectory of a rocket solely depends on stability. There are no measures in place to control thrust through fins actuation and thrust vectoring.
- The KNSU propellant exhibits lower efficiency compared to other propellants such as APCP. The KNSU has 20% less specific impulse (Isp) than the black powder charge.
- The data obtained from the sensors(PMS, DHT22) to the microcontroller has a low sampling rate.

5.5. Budget Analysis

The overall budget analysis for our project is presented below. This budget analysis provides a breakdown of the anticipated expenses for development, material procurement, manufacturing, testing, launch operations, and other associated costs.

Table 5.1: Budget Estimation

S. No.	Name of Particulars	Cost (Rs)
1	Electronics (Sensors, Processors, Batteries, etc.)	25,000/-
2	Body Fabrication	10,000/-
3	Booster Motor	20,000/-
4	Recovery Systems	6,000/-
5	Pressure Chamber	5,000/-
6	Thrust Stand modification	3,000/-
7	Launch Stand	8,000/-
8	Travel Expenses	35,000/-
9	Miscellaneous	10,000/-
	Total	122,000/-

CHAPTER 6: CONCLUSION

In summary, the construction of a full-scale model rocket encompassing components such as the main airframe, electronics bay, payload, and recovery systems was completed. The airframe was crafted using glass fiber composites to ensure structural strength and operational flexibility. The flight computer, incorporating MPU 6050 for acceleration and gyroscopic data, and BMP180 for pressure altitude and temperature data, served as the primary sensors.

Integration of the payload included the PMS5003t for particulate matter sensing and DHT22 for humidity and temperature sensing. Systems featuring ejection devices for recovery were developed and subjected to testing.

Static thrust stand tests were conducted in two phases, with general thrust values of 671 Newtons for a 45 mm motor and 1884 Newtons for a 57 mm motor, each serving different launch objectives. Depending on the grain configuration, observations revealed both neutral burning and progressive burning of the propellant, contributing to the characterization of the thrust curve.

Flight tests were carried out in two phases, yielding partial success. The initial test focused on body separation for recovery deployment, while the subsequent test concentrated on payload and recovery deployment at specific intervals. The integrated payload sensors operated at a low sampling rate of 1 Hz. With a flight duration of 12 seconds and limited altitude above ground level, the parachutes failed to fully deploy, impeding the attainment of terminal velocity and resulting in sparse atmospheric data samples.

In conclusion, a fully functional full-scale model rocket capable of executing its designated missions was designed and constructed. It possessed the capability to reach target altitudes, deploy payloads, and recover the body utilizing the recovery deployment system.

Scope for Future Enhancement

Prospective advancements in sounding rocket technology may center on propellant characterization beyond KNSU, investigating the integration of multi-stage Solid Rocket Boosters (SRB), and enhancing intricate systems such as fin actuation, thrust vector control, and landing leg mechanisms. Enhancing the rocket's propulsion system could be a focal point to elevate its apogee. Additionally, refining the airframe structure to decrease vehicle weight could potentially augment altitude capabilities.

References

[1] G. Seibert and B. T. Battrick, *The history of sounding rockets and their contribution to European space research*. ESA Publications division Noordwijk, 2006.

[2] G. P. Sutton and O. Biblarz, *Rocket propulsion elements*. John Wiley & Sons, 2016.

[3] L. Carvalho and G. Claudino, "Cfd analysis of drag force for different nose cone design," in *presented at the IX Forum de Pesquisa e Inovacao do Centro de Lancamento da Barreira do Inferno*, 2019.

[4] S. S. Sankalp, V. Sharma, A. Singh, A. S. Salian, and G. Srinivas, "Computational analyses of tail fin configurations for a sounding rocket," *Aerospace Systems*, vol. 5, no. 2, pp. 233–246, 2022.

[5] T. W. Knacke, "Parachute recovery systems design manual," Naval Weapons Center China Lake CA, Tech. Rep., 1991.

[6] A. Kräuchi, R. Philipona, G. Romanens, D. F. Hurst, E. G. Hall, and A. F. Jordan, "Controlled weather balloon ascents and descents for atmospheric research and climate monitoring," *Atmospheric measurement techniques*, vol. 9, no. 3, pp. 929–938, 2016.

[7] B. R. Brinley, *Rocket manual for amateurs*. Ballantine Books, 1960.

[8] R. A. Nakka, "Solid propellant rocket motor design and testing," Ph.D. dissertation, University of Manitoba, 1984.

[9] A. F. El-Sayed, *Fundamentals of aircraft and rocket propulsion*. Springer, 2016.

[10] J. Anderson, *EBOOK: Fundamentals of Aerodynamics (SI units)*. McGraw hill, 2011.

[11] K. Tejasvi, V. V. Rao, and Y. P. Setty, "Observation in ballistic evaluation motor static firing: Cracking in graphite nozzle," *International journal of scientific and engineering research*, vol. 8, pp. 1441–1446, 2017. [Online]. Available: https://api.semanticscholar.org/CorpusID:201321215

[12] F. Trevisi, M. Poli, M. Pezzato, E. Di Iorio, A. Madonna, N. Bressanin, and S. Debei, "Simulation of a sounding rocket flight's dynamic," in *2017 IEEE International Workshop on Metrology for AeroSpace (MetroAeroSpace)*. IEEE, 2017, pp. 296–300.

[13] E. Salente, "Preliminary sizing of parachute systems," Ph.D. dissertation, Politecnico di Torino, 2018.

[14] I. L. Vér and L. L. Beranek, *Noise and vibration control engineering: principles and applications*. John Wiley & Sons, 2005.

[15] G. H. Stine and B. Stine, *Handbook of model rocketry*. Wiley, 2004.

[16] J. D. Jacob, P. B. Chilson, A. L. Houston, and S. W. Smith, "Considerations for atmospheric measurements with small unmanned aircraft systems," *Atmosphere*, vol. 9, no. 7, p. 252, 2018.

[17] R. Kirchhartz, M. Hörschgen-Eggers, and W. Jung, "Sounding rockets are unique experimental platforms," 2018.

[18] M. P. Kunhikrishnan, "Opportunities for atmospheric studies through sounding rockets - unoosa.org," 2019. [Online]. Available: http://www.unoosa.org/documents/pdf/copuos/stsc/2019/tech-60E.pdf

[19] P. Wilkins, J. Henry, T. Hill, M. Buczkowski, O. Langrehr, O. Torres, and S. Pittaro, "Team 83 project report for irec 2018."

[20] M. Canepa, *Modern high-power rocketry*. Trafford Publishing, 2005, vol. 2.

[21] D. Poynter, "The parachute manual: a technical treatise on aerodynamic decelerators," *(No Title)*, 1991.

Appendices

Figure 6.1: Recovery System Test

Figure 6.2: Fiber Laying

Figure 6.3: Electronics Bay and Ejection Canister